# OSCILLATION AND CHAOS FOR INDUSTRIAL MECHATRONIC SYSTEMS

SUWILAI AREEJIT





A DISSERTATION SUBMITTED IN PARTIAL FULFILLMENT
OF THE REQUIREMENT FOR THE DEGREE OF
DOCTOR OF ENGINEERING IN ELECTRICAL ENGINEERING
FACULTY OF ENGINEERING
KING MONGKUT'S INSTITUTE OF TECHNOLOGY LADKRABANG
2014

KMITL-2014-EN-D-018-010

| | |
|---|---|
| **หัวข้อวิทยานิพนธ์** | การใช้ความผันผวนและความอลวนในระบบอิเล็กทรอนิกส์เชิงกลอุตสาหกรรม |
| **นักศึกษา** | นายสุวิไล อารีจิตต์ |
| **รหัสประจำตัว** | 52610136 |
| **ปริญญา** | วิศวกรรมศาสตรดุษฎีบัณฑิต |
| **สาขาวิชา** | วิศวกรรมไฟฟ้า |
| **พ.ศ.** | 2557 |
| **อาจารย์ที่ปรึกษาวิทยานิพนธ์** | รศ.ดร.ปิติเขต สู้รักษา |

## บทคัดย่อ

เสถียรภาพของระบบพลศาสตร์โดยทั่วไปจะขึ้นอยู่กับตัวแปรและปัจจัยหลากหลาย ความผันผวนของตัวแปรเพียงเล็กน้อยสามารถสร้างผลกระทบต่อระบบได้เป็นอย่างมาก ปรากฏการณ์ลักษณะดังกล่าวสามารถเกิดขึ้นได้กับทุกระบบ และมีทฤษฎีที่เกี่ยวข้องกับพฤติกรรมนี้คือ “ทฤษฎีความอลวน” การประยุกต์ใช้ทฤษฎีความอลวนโดยส่วนมากจะเป็นการจำลองและศึกษาพฤติกรรมของระบบ ส่วนการประยุกต์ใช้งานจริงในวงการอุตสาหกรรมยังไม่เป็นที่แพร่หลาย วิทยานิพนธ์ฉบับนี้จึงเสนอวิธีการใหม่ในการนำการแกว่งและความอลวนมาใช้ประโยชน์ในเชิงพาณิชย์ พร้อมทั้งเสนอวิธีการประยุกต์ใช้กับระบบอิเล็กทรอนิกส์เชิงกลในงานอุตสาหกรรม การแกว่งในการทดลองมีสองลักษณะคือการแกว่งแบบรายคาบและแบบอลวน โดยการแกว่งแบบรายคาบสร้างจากส้อมเสียงที่ติดเพียโซอิเล็กทริกเรโซเนเตอร์ขนาดเล็กซึ่งสามารถนำไปวิเคราะห์คุณลักษณะของวัสดุในระดับไมโครเมตรถึงนาโนเมตรได้อย่างละเอียดแม่นยำ ส่วนการแกว่งแบบอลวนจะนำไปใช้ในการสร้างโหมดการแพร่กระจายคลื่นไมโครเวฟเพื่อให้ความร้อนกระจายทั่วถึงภายในเตาปฏิกรณ์ โดยปราศจากชิ้นส่วนอุปกรณ์ที่มีการเคลื่อนไหวเชิงกล ทำให้สามารถลดต้นทุนการสร้างเครื่องจักรได้

| | |
|---|---|
| **Thesis Title** | Oscillation and Chaos for Industrial Mechatronic Systems |
| **Student** | Mr.Suwilai Areejit |
| **Student ID.** | 52610136 |
| **Degree** | Doctor of Engineering |
| **Program** | Electrical Engineering |
| **Year** | 2014 |
| **Thesis Advisor** | Assoc.Prof.Dr.Pitikhate Sooraksa |


## ABSTRACT

The stability of a dynamic system is subject to many parameters and even a slight change in the initial parameters can induce significant variations in the system. The phenomena are present in all systems and are termed "chaotic theory". The current applications of the chaotic theory are concerned largely with the modeling and study of the system behavior but minimally with the large scale industry. This dissertation thus deals with the commercial-scale application of the novel methods that use both oscillation and chaotic phenomena to industrial mechatronic systems. In the experiment there are two types of oscillation, i.e. periodic oscillation and chaotic oscillation. The periodic oscillation is generated with the tuning fork and the small piezoelectric, which can be utilized in classification and analysis of the micro-scale to nano-scale materials. Meanwhile, the chaotic oscillation is used in the design of the microwave propagation pattern to guarantee uniform internal heat distribution without the stirring mechanism to reduce the construction cost and complexity of the reactor.

# Acknowledgments

This dissertation could not have materialized were it not for the financial support from the Thailand Research Fund under the RGJ-PhD/131/2551 grant and the National Innovation Agency (NIA) of Thailand's Ministry of Science and Technology under the biomass carbonizer project (P11-EN-52-03-003). In addition, the support and assistance from Prommark Co., Ltd. and Vision Zone Co., Ltd. contributed to the completion of this research.

I am deeply indebted to my advisor, Associate Professor Dr. Pitikhate Sooraksa, for his patiently guiding me toward the right path to the completion of my dissertation. I would also like to express my sincere appreciation to Associate Professor Dr. Sombat Teekasap for his encouragement and to Professor Dr. Hisayuki Aoyama and Jing Xiaobei of the AOLAB at the University of Electro-Communications, Japan, for assistance and suggestions.

Furthermore, my sincere gratitude goes to my parents, grandparents, spouse, siblings, Assistant Professor Dr. Kitdakorn Klomkarn, Ajarn Vichit Lohprapan, Dr. Poomyos Payakkawan, and Dr. Anurak Jansri, without whom this dissertation would not have completed.

Suwilai Phumpho (Areejit)

# TABLE OF CONTENTS

# TABLE OF CONTENTS (cont.)

# LIST OF FIGURES

# LIST OF FIGURES (cont.)

# LIST OF FIGURES (cont.)

# LIST OF TABLES

# Chapter 1
# Introduction

## 1.1 Background

For the past few decades, import of industrial machinery and equipment has accounted for highest import values of the Kingdom of Thailand. To reduce the dependence on machinery imports, it is necessary that Thailand develop home-grown technologies and machines. Many organizations in public and private sectors as well as academic institutions thus fund research studies in the development of the technologies appropriate for industrial applications in the Kingdom to strengthen the nation's economy. This dissertation is thus concerned with the development of a home-grown industrial-scale machine using the oscillation technology.

Oscillations are ubiquitous phenomena and can be found in, for instance, mechanical vibrations, electrical signals, chemical reactions, biological interactions, human body, economy, weather. An oscillation is a disturbance in a physical system that is both repetitive in time and periodic in space [1]. The oscillation phenomena are generally encountered in dynamic systems, which can be explained by differential equations and iterated maps [2]. Differential equations describe the evolution of systems in continuous time, whereas iterated maps arise when time is discrete. Most research studies on oscillations in engineering have tried to maintain the stability of dynamic systems; however, chaotic behaviors still occur in the dynamic systems, whose sensitivity depends on the initial condition [3]. In addition, the research was conducted using modeling and simulation and on a pilot scale [4-8]. Nevertheless, the experiments of this dissertation are of an industrial scale.

This dissertation is concerned with the application of mechanical or periodic oscillation and chaotic oscillation on an industrial scale. The simple mechanical oscillation is used to classify materials in a nanometer level, while the chaotic oscillation is adopted in the design of microwave radiation to generate a uniform heating distribution in a reactor and thus no stirring mechanism is required. The experiments are thus divided into the applications of periodic oscillation and of chaotic oscillation.

### 1.1.1 Periodic oscillation application

An image processing method is a common method adopted to classify the materials and the performance of the method depends on the material size, light source, focus length, and mechanical part movement [9-12]. In the mechanical part movement control, it is very difficult to achieve in the scale of nanometer. In addition, nano-scale sensing devices are costly and require advanced skills to calibrate [13].

Although the image processing method is nondestructive, it is unsuitable for elastic nano materials [14]. To overcome, a quartz tuning fork (QTF), a basic device in the atomic force microscopy (AFM), is used. The QTF in this dissertation consists of a tuning fork and a piezoelectric and is a mechanical oscillator excited by the piezoelectric actuator at the resonance frequency.

The QTF with a tiny probe tip typically has a measurement range of 1-100 nm suitable for nano-scale sensing applications [15-17] and can be applied economically to mechanical movement sensing. The QTF measurement precision is subject to the size and shape of the probe tip. Due to unavailability of commercial probes suitable for material classification, the needle probes are manually produced and thereby impact the precision of measurement [18]. To address this problem, the amplitude requires adjustment by adjusting the driving voltage. The adjusted amplitude is then applied to the QTF at the resonance frequency to increase the Quality ($Q$) factor. As a result, the QTF mechanical vibration is a function of $Q$ factor [19,20].

The QTF with a mounted needle is capable of producing precise and reliable measurements for classification of nano-scale materials. The technique is also repeatable.

### 1.1.2 Chaotic oscillation application

In the conventional industrial heating or surface heating process, the process time is constrained by the heat flow rate from the surface into the material core, which is subject to the material specific heat, thermal conductivity, density and viscosity. The heat distribution is not only slow but also non-uniform as the temperatures of the material surface, edges and corners are higher than the material

core [21]. The heating mechanism with microwave energy is very different from the conventional heating. Microwave is not a form of heat but rather of energy that is manifested as heat through its interaction with materials by exciting the outer layers of the material molecules. The inner of the materials is warmed as heat travels inward from the outer layers [22,23]. Most microwave heating systems have a stirring mechanism for even radiation of microwave inside the reactor; however, certain industrial applications require a microwave heating system without stirring mechanism to reduce the development and maintenance costs. To achieve this goal, chaotic behavior is applied to the microwave heating system without stirring mechanism. The chaotic behavior is found in both household electrical appliances, e.g. dishwashers, air conditioners, heaters, and microwave ovens [24-26]; and industrial applications, e.g. chaotic mixing [27,28], and chaotic compaction [29]. However, the chaotic microwave heating has not been employed on an industrial scale. The simple chaotic oscillations are used to generate chaotic microwave radiation patterns to induce the uniform heating distribution inside the reactor. This reduces the processing time and guarantees an even distribution of heat inside the reactor with no complex mechanism required. In addition, this proposed technique is a good alternative to the conventional heating system.

## 1.2 Objectives

The objectives of this dissertation are as follows:

(1) To model the mechanical oscillator with computer simulation;

(2) To apply the mechanical oscillator to classification of materials;

(3) To simulate chaotic patterns with computer simulation;

(4) To apply the chaotic patterns to industrial microwave heating without stirring mechanism;

(5) To apply the oscillation behavior on an industrial scale.

## 1.3 Research scope

The scope of this dissertation includes the applications of periodic and chaotic oscillations and the simulation of the oscillations. The periodic oscillation is generated by a mechanical oscillator for classification of the materials. The mechanical oscillator in the experimentation is a tuning fork with a piezoelectric resonator, which is termed the tuning fork with piezoelectric (TFP). The TFP is a basic device with high accuracy suitable for classification of nano materials. The basic principles of TFP can be simulated by a mechanical model or an electrical model. An increase in the mass of tuning fork after the mounting of a needle initially reduces the $Q$ factor, which requires a tuning of $Q$ factor by a software program and an addition of electronic components to improve the $Q$ factor.

The chaotic oscillation is generated by a simulation program, and the chaotic behaviors are confirmed by Lyapunov exponents and bifurcation diagrams. Positive Lyapunov exponents indicate the chaotic behavior while the Bifurcation diagrams identify suitable parameters for generation of chaotic patterns. One of the chaotic patterns is selected and applied to a biomass carbonation process using the multi-feed microwave heating without stirring mechanism. The heating temperature of the proposed method is compared with that of the conventional microwave heating method.

## 1.4 Contributions

The contributions can be divided into two main areas, i.e. those to the industrial-scale periodic oscillation and to the commercial-scale chaotic oscillation.

### 1.4.1 Contributions to the periodic oscillation

(1) Elastic nano materials classification application.

(2) Nano-scale mechanical movement sensing application.

### 1.4.2 Contributions to the chaotic oscillation

(1) Chaotic patterns for multi-feed microwave heating.

(2) Industrial microwave heating without stirring mechanism.

## 1.5 Dissertation outline

The organization of this dissertation is as follows:

Chapter 1 outlines the introduction, objectives, research scope and contributions of this dissertation.

Chapter 2 is an overview of oscillations in nature and types of oscillations. It also discusses the mechanical oscillator.

Chapter 3 explains the chaos theory and methods to indentify chaotic behaviors. Chaotic equations are presented in the chapter and applied to chaos engineering.

Chapter 4 details the mechanical oscillator or tuning fork for sensing application. The tuning fork with piezoelectric is introduced for classification of the nano-scale materials.

Chapter 5 discusses the chaotic application for industrial microwave heating. It also details the chaotic pattern generation and the impacts of chaotic behavior on an operable multi-feed microwave heating without stirring mechanism.

Chapter 6 is the conclusions, contributions and future works.

# Chapter 2

# Oscillation

## 2.1 Introduction

Oscillations are systems with observables whose time evolutions remain bounded and fluctuate around certain equilibrium value. Since the behavior is often found in many scientific disciplines, such as natural sciences, medicine, engineering, the study of physics and mathematics of oscillations has become a scientific fundamental. Periodicity associated with astronomical events was among the first natural phenomena described with such sufficient precision and generality that future similar events could be predicted. This early success in describing and predicting the periodic astronomical events together with an understanding of periodicity related to sound-producing vibration led scientists to seek periodicities elsewhere in the nature. Explanations of sound, tone, and harmonics were among the first elements of modern physical science. The list of phenomena in which cycles have been studied is becoming extensive. It includes sunspot activity, tides and ocean waves, earth tides, music, human speech, tree-ring growth, animal population changes, brain waves, heart rhythm, chemical bonding forces, climatic activity, economic growth, light and other electromagnetic wave phenomena, and geological events [30,31].

A common feature of the study of periodicity in natural phenomena is the search for the more important cycle periods or cycle frequencies. An attempt then is made to explain the cycles in terms of more fundamental phenomena. The classic method of harmonic analysis has been used to determine these cycles. No general method exists for relating the detected cycles to other phenomena. Recently, a new approach has been taken to the study of oscillatory phenomena in which concepts of statistics have been applied to a generalized harmonic analysis theory, allowing periodicities to be detected in the presence of noise. Noise is defined as oscillation of the value of a variable without any periodicity. Where periodicities as well as the random variation are present in a variable, the cyclic component may be obscured unless some means is adopted to separate or filter out the noise. Figure 2.1 shows three types of oscillation: (a) periodic, (b) random, and (c) chaotic oscillations containing periodic and random variations. Examples of the last type of oscillation are

tree-ring width, an economic index such as gross national product, an electronic signal, or height of water in a basin subject to wave action [32].

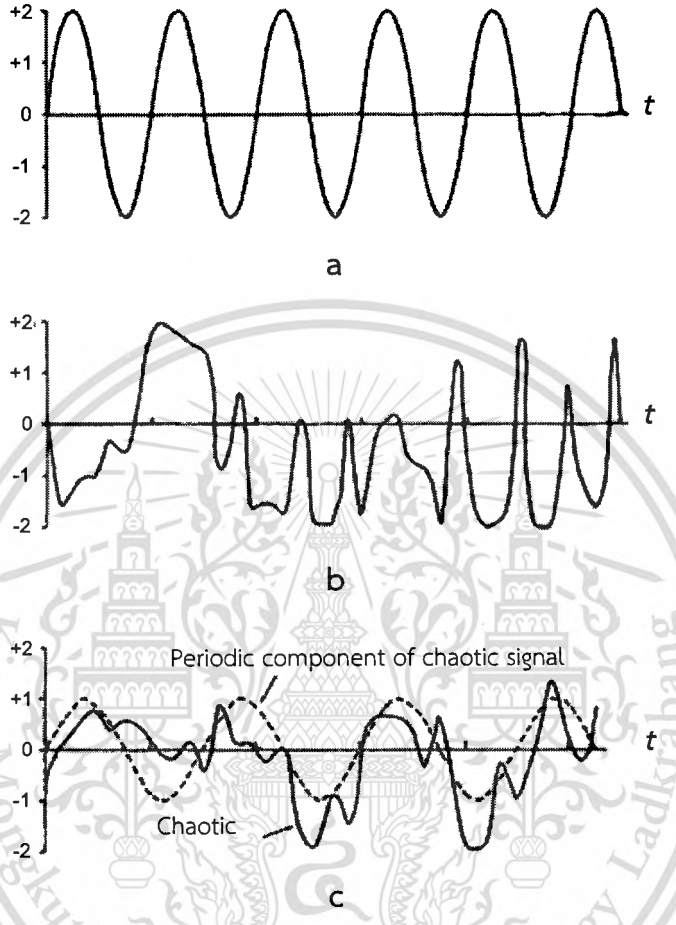


**Fig. 2.1** Types of oscillatory behavior: (a) periodic oscillation, (b) random oscillation devoid of periodic component, and (c) chaotic oscillations containing periodic and random variations [32].

A simple and meaningful type of oscillation is the harmonic oscillator which displays a periodic behavior. This is a nonlinear system whose theoretical study can be carried out by standard mathematical techniques, and almost describes the oscillations that occur in nature. In the most relevant applications of the physics of oscillations, these oscillators are not isolated entities but are subsystems of the interaction with an environment. There are two basic relevant scenarios of oscillators: oscillators being driven from their surroundings and mutually coupled oscillators.

## 2.2 Oscillation phenomena

Most oscillatory phenomena seem to possess both random (noisy) and periodic components. The methods of separating noise from periodic signals are now reasonably developed within the field of electrical communications. Even with the application of these methods, it is not always possible to completely separate the desired periodic portion from the noise. However, the generalized theory of harmonic analysis makes it possible to quantitatively present a particular sample of a composite periodic signal and the noise to any desired degree of accuracy. This combined oscillatory signal represents only the observed portion of the phenomenon but not represents the totality of the separate periodic and random components. In a sense, it could be said that this sample of the combined signal contains all the available information of the phenomenon, assuming no other sample is available. This requires a minimal set of numbers to represent this signal sample. The set of numbers should be minimal in the sense that it takes fewer numbers to represent the signal than those contained in the original signal. It will be shown that through a Fourier analysis a set of numbers is extractable for a given signal under proper circumstances. This set of numbers is an appropriate descriptor of the phenomenon, and is the number set that can distinguish members of one class from those in another class [32]. Table 2.1 presents examples of oscillations.

**Table 2.1** Examples of oscillations

| | | |
|---|---|---|
| 1. | Mechanical | Tuning fork, Pendulum, Helmholtz resonator |
| 2. | Electrical | RLC circuit, Oscillator, Chaotic circuit |
| 3. | Electro-mechanical | Crystal oscillator, Microphone, Loudspeaker |
| 5. | Biological | Population growth, Circadian rhythm, Oscillating gene |
| 6. | Human | Neural oscillation, Cardiac rate, Breathing rate |
| 7. | Economic and social | Business cycle, Generation gap, Stock exchanges |
| 8. | Climate and geophysics | Weather, Atlantic multi-decadal ,Pacific decadal |
| 9. | Astrophysics | Neutron stars, Cyclic model |
| 10. | Chemical | Chemical reaction, Chemical mixing |

## 2.3 Harmonic oscillator

A simple harmonic oscillator is a mass connected to some elastic object of negligible mass that is fixed at the other end and constrained so that it may only move in one dimension. Many vibration and oscillation systems can be approximated by this simplified model. The problem of approximation with the simplified model, however, lies in the fact that the equations of a similar form arise when a particle moves through any region whose potential has one or more local minima. The simple harmonic oscillator, e.g. in the planetary and satellite motion, an electron in orbit around a nucleus, pendulums, is similar to RLC circuits [33].

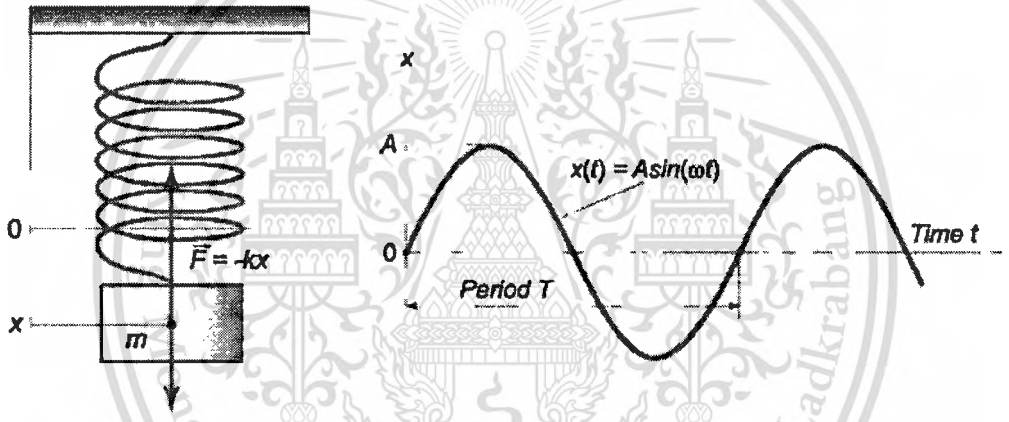


Fig. 2.2 Harmonic oscillations [33]

An example of the simple system is the mass *m* attached to a spring of stiffness k as shown in Figure 2.2 In an ideal case (ignoring air resistance and friction), the system will perform undammed harmonic oscillations, in which the displacement *x* is described by the cosine or sine function:

$$x(t) = A\cos(\omega t + \varphi_0) \tag{2.1}$$

$$x(t) = A\sin(\omega t + \varphi_0) \tag{2.2}$$

where A denotes the amplitude of oscillation, $\omega t + \varphi_0$ is the phase of oscillation, $\varphi_0$ is the initial phase at time $t$ = 0. The variable $\omega$ is called the circular or cyclic frequency of oscillation. It is related to the period of oscillation $T$ by the formula:

$$\omega = \frac{2\pi}{T} \tag{2.3}$$

If the displacement $x(t)$ is known, then sequentially differentiating Eq.(2.1), we can find the velocity and acceleration of the body:

$$v(t) = \dot{x}(t) = A\omega \sin(\omega t + \varphi_0) \tag{2.4}$$

$$a(t) = \ddot{x}(t) = \dot{v}(t) = A\omega^2 \cos(\omega t + \varphi_0) \tag{2.5}$$

This shows that the displacement $x(t)$ and acceleration $\ddot{x}(t)$ satisfy the differential equation:

$$\ddot{x} + \omega^2 x = 0 \tag{2.6}$$

which is the equation of harmonic oscillations. The solution of this equation is mentioned in cosine or sine functions. In the case of a mass on a spring, the restoring force for small oscillations obeys Hooke's law:

$$F = -kx \tag{2.7}$$

Where $k$ is the stiffness of the spring. Here the coordinate $x = 0$ corresponds to the point of equilibrium, in which the force of gravity is balanced by the initial tension of the spring. Then, according to Newton's second law, the movement of the mass will be described by the differential equation:

$$m\ddot{x} = -kx \tag{2.8}$$

$$\ddot{x} + \frac{k}{m}x = 0 \tag{2.9}$$

Thus, the mass on the spring will perform undammed harmonic oscillations with circular frequency:

$$\omega = \sqrt{\frac{k}{m}} \tag{2.10}$$

The period of oscillation will be equal to:

$$T = \frac{2\pi}{\omega} = 2\pi\sqrt{\frac{m}{k}} \tag{2.11}$$

## 2.4 Tuning fork

A tuning fork is an acoustic resonator in the form of a two-pronged fork with the prongs (tines) formed from a U-shaped bar of elastic metal (usually steel). It resonates at a specific constant pitch when set vibrating by striking it against a surface or with an object, and emits a pure musical tone after awaiting a moment to allow for some high overtones to die out. The pitch that a particular tuning fork generates depends on the length and mass of the two prongs. It is frequently used as a standard pitch to tune musical instruments [34].

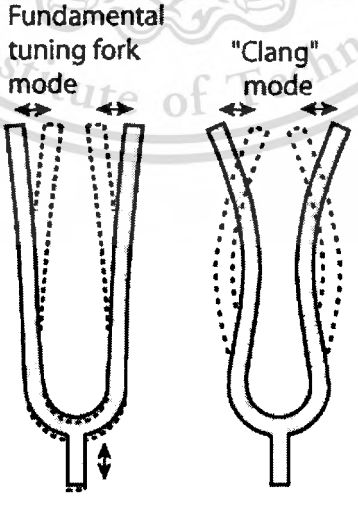


**Fig. 2.3** The tuning fork mode [34]

The tuning fork has a very stable pitch and has been used as a pitch standard since the Baroque period. The "clang" mode has a frequency which depends upon the details of construction, but is usually 6 times above the fundamental frequency, as exhibited in Figure 2.3. This is close to the first overtone of the clamped bar. The clang tone dies away rapidly. The two sides or "tines" of the tuning fork vibrate at the same frequency but move in opposite directions at any given time. The two generated sound waves will show the phenomenon of sound interference. The frequency of a tuning fork depends on its dimensions and the material from which it is made: [35]

$$f = \frac{1.875^2}{2\pi l^2}\sqrt{\frac{EI}{\rho A}} \tag{2.12}$$

where:

$f$ is the frequency the fork vibrates (in Hertz)

$l$ is the length of the prongs in meters.

$E$ is the Young's modulus of the material the fork is made from in pascals.

$I$ is the second moment of area of the cross-section in metres to the fourth power.

$\rho$ is the density of the material the fork is made from in kilograms per cubic meter.

$A$ is the cross-sectional area of the prongs (tines) in square meters.

## 2.5 Quartz tuning fork (QTF)

The basic principle of the tuning fork [35-39] is commonly known to musicians: two prongs connected at one end make a resonator whose resonance frequency is defined by the properties of the material from which it is made and by its geometry. Although each prong can be individually considered as a first approximation to analytically determine the available resonance frequencies, the symmetry of the two prongs in a tuning fork reduces the number of possible modes with a good quality factor [40]. An input port is excited by sinusoidal wave at the

specific frequencies; simultaneously an output port can be measured by the responses of the QTF. In order to obtain the specific frequencies of each QTF, the mechanical model [41] and the electrical model [42] are generally used with the specific parameters.

The resonance model of the QTF is described by a Butterworth-Van Dyke equivalent circuit: a resistance is acoustic losses in material and environment, inductor is a mass, and a capacitor is stiffness. The similar quantities between the mechanical and electrical models are presented in Figure 2.4. Typical values are $C_s \approx 5\rho F$ and $C \approx 0.01\rho F$, yielding an inductance value $L$ in the $kH$ range and a motional resistance in the $k\Omega$ range. The unique property of quartz resonator is a huge equivalent inductance in a tiny volume [43]. The mechanical model of resonator, as a damped oscillator and an electrical oscillator model, includes the motional mechanical equivalent series circuit in parallel with the electrical capacitance between the electrodes separated by the quartz substrate branch. Summary of the equivalent quantities between the mechanical and electrical models is presented in Table 2.2.

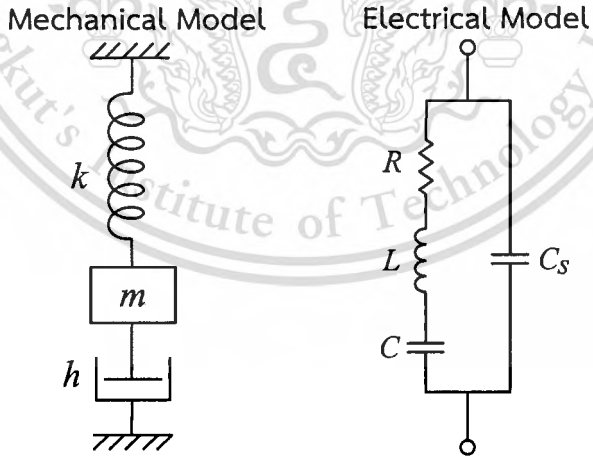


**Fig. 2.4** The mechanical and electrical models of a tuning fork oscillator. $C_s$ is the parasitic capacitance of the tuning fork [43].

**Table 2.2** The QTF parameters of the mechanical and electrical models [43]

| Mechanical Model | Electrical Model |
|---|---|
| $h$ (friction) | $R$ (resistance) |
| $M$ (mass) | $L$ (inductor) |
| $k$ (stiffness) | $1/C$ (capacitance) |
| $x$ (displacement) | $q$ (electrical charge) |
| $\dot{x}$ (velocity) | $i = dq/dt$ (current) |
| $m\ddot{x} + h\dot{x} + kx = F$ | $L\ddot{q} + R\dot{q} + q/C = U$ |
| $Q = 1/h\sqrt{km}$ | $Q = 1/R\sqrt{L/C}$ (quality factor) |
| $\omega_0 = \sqrt{k/m}$ | $\omega_0 = 1/\sqrt{LC}$ (angular frequency) |

The tuning fork can be modeled simply as a driven harmonic oscillator and electrically by the Butterworth-Van-Dyke equivalent circuit. Starting with the equation of motion for a simple harmonic oscillator [44],

$$m\ddot{x}(t) + kx(t) = 0 \tag{2.13}$$

where $m$ is the mass of the system and $k$ is the spring constant. Building upon this equation and factoring in the driving force for the oscillator and a damping force acting on the oscillator gives a more accurate equation for the oscillation of a tuning fork as a driven oscillator with damping,

$$m\ddot{x}(t) + b(\dot{x}) + kx(t) = F_0 \cos(\omega t) \tag{2.14}$$

where $b$ is the viscous damping factor and $F_0 \cos(\omega t)$ is the sinusoidal driving force for the tuning fork. The tuning fork can also be modeled by a similar second-order differential equation. The electrical equivalent is the Butterworth-Van-Dyke equation, given by,

$$L\ddot{I}(t) + R\dot{I}(t) + \frac{1}{C} I(t) = U \cos(\omega t) \tag{2.15}$$

where $L$ is inductance, $R$ is resistance, $C$ is capacitance, and $U$ the potential added to the oscillator. This equation can also be obtained using Kirchhoff's law of conservation of energy. The steady-state amplitude solution for a driven-damped harmonic oscillator is

$$X(t) = \frac{F_0}{\sqrt{b^2\omega^2 + m^2(\omega_0^2 - \omega^2)^2}} \cos(\omega t) \tag{2.16}$$

where the phase is given as

$$\tan\varphi = \frac{b\omega}{m(\omega_0^2 - \omega^2)} \tag{2.17}$$

The resonance condition for free oscillation frequency including damping is

$$\omega_0 = \sqrt{\frac{k}{m}} \tag{2.18}$$

The quality factor of the tuning fork oscillator can be defined by the constants in the system, both mechanical and electrical.

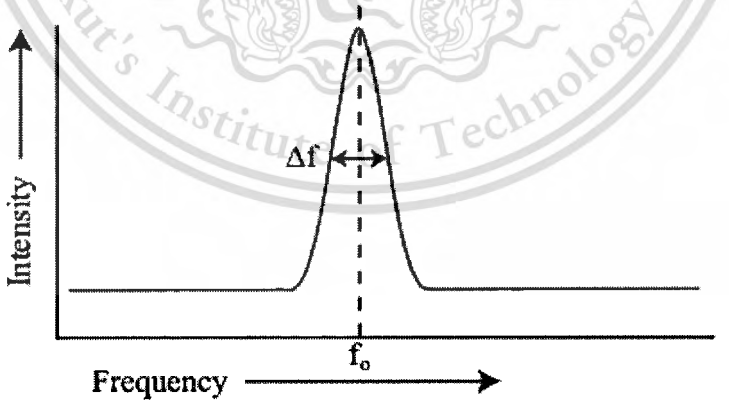


**Fig. 2.5** The measurement of quality factor based on the amplitude and frequency response of the tuning fork.

A qualitative measurement of the full-width at half-maximum (FWHM) of the oscillator as seen at resonance frequency can also be used to calculate the quality

factor. Figure 2.5 demonstrates the qualitative measurement of the FWHM of a resonator. The relationships between these parameters are given by

$$Q = \frac{f_0}{\Delta f} = \sqrt{\frac{mk}{b}} = \frac{1}{R}\sqrt{\frac{L}{C}} \tag{2.19}$$

Incorporating the quality factor into the steady-state solution will allow the effect of quality factor on the response time of the oscillator to be examined. We include $Q$ by substituting for $b$, including the resonance condition for the free oscillation damping. The amplitude is given by

$$x_0 = \frac{F_0/m}{\sqrt{\left(\frac{\omega_0\omega}{Q}\right)^2 + (\omega_0^2 - \omega^2)^2}} \tag{2.20}$$

with the phase defined as

$$\varphi_0 = \tan^{-1}\left[\frac{\omega_0\omega}{Q(\omega_0^2 - \omega^2)}\right] \tag{2.21}$$

If the amplitude $x_0$ is changed by a perturbation, the amplitude and phase become terms in the general solution

$$X(t) = x_0 \cos(\omega t + \varphi_0) \tag{2.22}$$

The introduction of an instantaneous frequency change gives a solution with a steady state and transient term:

$$X(t) = \dot{x}_0 \cos(\omega t + \dot{\varphi}_0) + x_t e^{\left(-\frac{\dot{\omega}_0 t}{2Q}\right)} \cos(\omega t + \varphi_t) \tag{2.23}$$

The time constant for the transient term gives the settling time for the amplitude, and ultimately the response time of the quartz oscillator. The time constant in terms of quality factor and frequency is given by

$$\tau = \frac{2Q}{\omega_0} \tag{2.24}$$

## 2.6 Summary

A tuning fork is a simple mechanical oscillator that can generate a specific resonance frequency after a tiny piezoelectric device (i.e. quartz) is attached onto the prong of the tuning fork, the product of which is a quartz tuning fork (QTF). The QTF is vibrated by small oscillating voltages applied to the metal electrodes on the quartz crystal surface. The small oscillating voltages are generated by an electronic oscillator circuit. Generally, the operating principle of QTF can be demonstrated with either a mechanical or electrical model. However, this research work did not employ the mechanical model. In the electrical model, a QTF is used for material classification based on the distance and phase trajectory of QTF after its coming into contact with the material surface. More details on the electrical model of QTF are in Chapter 4. The next chapter (Chapter 3) discusses types of chaotic map, Bifurcation and the usefulness of Lyapunov exponents for identifying chaotic systems.

# Chapter 3
# Order to chaos

## 3.1 Introduction

The stability of a dynamic system is generally dependent on several parameters. A small change of the oscillation can result in large differences in the system. This phenomenon which occurs with every system leads to the study of chaos and the establishment of "chaotic theory". The chaotic theory is a field of study in mathematics, with applications in several disciplines including meteorology, physics, engineering, economics and biology. The theory studies the behavior of dynamical systems that are highly sensitive to initial conditions, a phenomenon which is commonly referred to as the butterfly effect. The small differences of initial conditions yield widely diverging outcomes for such dynamical systems, and it is impossible to predict a rendering in the long term [45]. The effect is deterministic, meaning that their future behavior is fully determined by their initial conditions, with no random elements involved [46]. In other words, the deterministic nature of these systems does not make them predictable [47,48]. This behavior is known as deterministic chaos, or simply chaos.

Sensitivity to initial conditions is commonly known as the "butterfly effect", which is so called because of the title of a paper given by Edward Lorenz in 1972 to the American Association for the Advancement of Science in Washington, D.C., titled *Predictability: Does the Flap of a Butterfly's Wings in Brazil set off a Tornado in Texas?* The flapping wing represents a small change in the initial condition of the system, which causes a chain of events leading to large-scale phenomena. The consequence of sensitivity to initial conditions manifests that if we start with only a finite amount of information about the system, then beyond a certain time the system will no longer be predictable [49].

The most fundamental property of a linear system is the validity of the principle of superposition. A nonlinear system does not hold the superposition principle. Nonlinearity is an undesirable phenomenon in a system and should exist as little as possible in the system. Let us take any linear time invariant system in this world, we can find some nonlinearities in that system up to certain extent. Unfortunately, there is a difficulty in evaluating the stability of a nonlinear system.

The perfect linear systems do not exist in practice since all practical systems are nonlinear to some degree. Similar to many terms in science, there are no standard definitions of chaos. Nevertheless, chaotic behavior has some typical features as follows [50]:

- **Nonlinearity:** Nonlinearity is a necessary, however not sufficient, condition for the occurrence of chaos. A chaotic system does not need to be very complex. For example, $f(x) = ax(1-x)$ is relatively simple, but it does need to be nonlinear. Essentially, all realistic systems exhibit certain degrees of nonlinearity.
- **Determinism:** Chaos must follow one or more deterministic equations that do not contain any random factors. The system states of past, present and future are controlled by deterministic, rather than probabilistic, underlying rules. Practically, the boundary between deterministic and probabilistic systems may not be so clear since a seemingly random process might involve the deterministic underlying rules that are yet to be found.
- **Sensitivity to initial conditions:** A small change in the initial state of the system can lead to extremely different behavior in its final state. Thus, the long term prediction of system behavior is impossible even though it is governed by deterministic underlying rules.

**Table 3.1** History of dynamics and chaos

| | | |
|---|---|---|
| 1666 | Newton | Invention of calculus, explanation of planetary motion |
| 1700 | | Flowering of calculus and classical mechanics |
| 1800 | | Analytical studies of planetary motion |
| 1890 | Poincaré | Geometric approach, nightmare of chaos |
| 1898 | Jacques Hadamard | Particle trajectories diverge exponentially from one another |

| | | |
|---|---|---|
| 1950-1960 | Birkhoff<br>Kolmogorov<br>Arnol'd<br>Moser | Complex behavior in Hamiltonian mechanics |
| 1963 | Edward Lorenz | Chaos in weather predictions and found strange attractor in simple model of convention |
| 1970 | Ruelle and Takens | Turbulence and chaos |
| 1974 | May | Chaos in logistic map |
| 1975 | Li and Yorke | Period three implies chaos |
| 1978 | Feigenbaum | Universality and renormalization, connection between chaos and phase transitions |
| 1982 | Mandelbrot | Fractals |
| 1983 | Chua | Chua's circuit is a simple electronic circuit |
| 1990 | Ott, Grebogi , and Yorke | Control of chaos |
| 1997 | Chen | Anticontrol of chaos |

## 3.2 One-dimensional maps

One-dimensional maps (sometimes called difference equations or iterated maps or recursion relations) are mathematical systems that model a single variable as it involves over discrete steps in time. One-dimensional maps come from [51]:

- Modeling natural phenomena such as population dynamics, electronics, economics, etc.
- Simple examples of chaos.

Examples of simple one-dimensional maps are listed here and again shown in Figure 3.1.

- The logistic map

$$f(x) = ax(1-x) \qquad (3.1)$$

$$;0 \le a \le 4$$

- The tent map

$$f(x)=\begin{cases} ax & ,x<\frac{1}{2} \\ a(1-x) & ,x>\frac{1}{2} \end{cases} \qquad (3.2)$$

$$;0\le a\le 2$$

- The shift map

$$f(x)=2x \bmod 1 \qquad (3.3)$$

- The sine map

$$f(x)=\frac{a}{4}\sin(\pi x) \qquad (3.4)$$

$$;0\le a\le 4$$

It is conventional to scale variables so that the interval $0\le a\le 1$ is mapped into itself. The ranges of control parameter $a$ are the limits when this condition is satisfied.

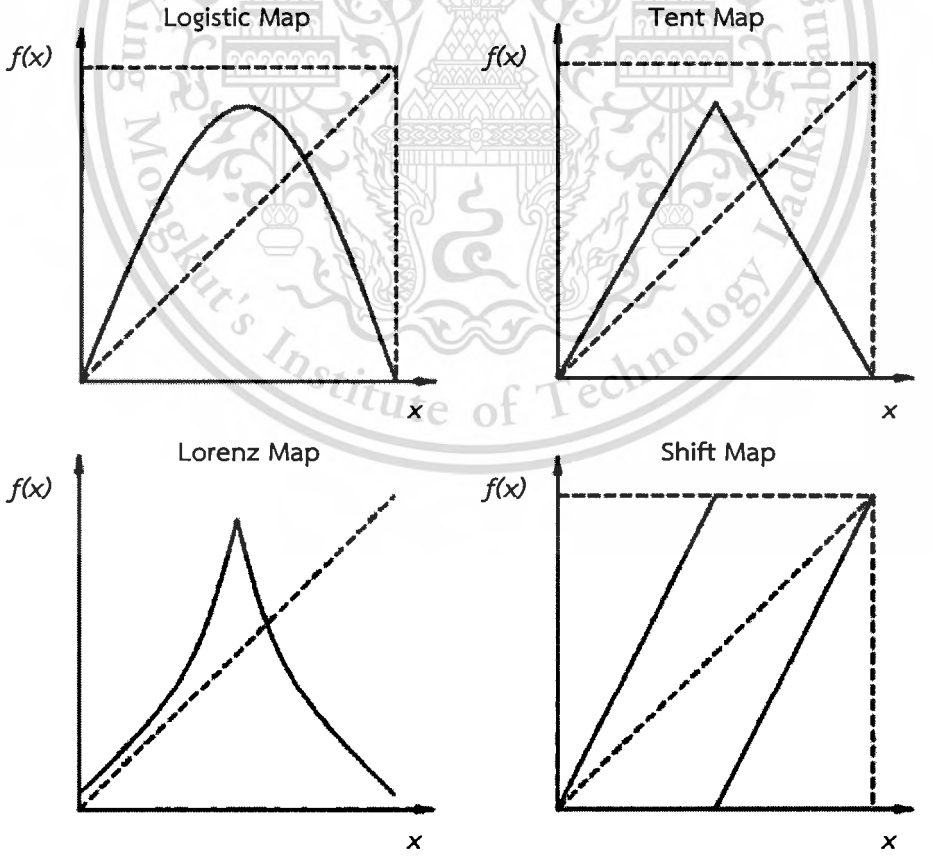


**Fig. 3.1** The examples of one-dimensional maps [51]

The iteration of one-dimensional map is easy to see graphically. If we plot $f(x)$ and $y = x$, the iterations are given by successive steps between these two curves:

$$y = f(x), \; x_{n+1} = y \tag{3.5}$$

Successive iterations from a given initial value are determined by successive operations of the map, an operation known as the "functional composition":

$$\begin{aligned} x_1 &= f(x_0) \\ x_2 &= f(x_1) = f(f(x_0)) \\ &\vdots \\ x_n &= f(x_{n-1}) = f(f \ldots (x_0)) \end{aligned} \tag{3.6}$$

## 3.3 Bifurcation

As the map parameter changes, the characteristic of a longer period bifurcation may dramatically change, e.g. from a fixed point to a period of two limit cycles. These changes are called bifurcations. The bifurcations that occur, and the different types of orbits, are best presented by a "bifurcation map". This is constructed with the parameter $a$ along the abscissa, and all values of $x$ visited after some number of iterations to eliminate transients plotted as points along the ordinate. A fixed point orbit over a range appears as a single curve, which splits into two curves at the bifurcation and enters period 2. The two curves then splits into four curves before entering period 4. The number of split curves at the bifurcation increases by $2^n$ to infinity. Chaotic dynamics, where the orbit visits and revisits an infinite number of points and thereby becomes periodic, appears as bands of continua of points [52].

The bifurcation maps of one-dimensional maps show that even very simple dynamical systems produces an excellent bifurcation structure. This complexity of the bifurcation of the Logistic map was studied by May [53] in the context of population dynamics.

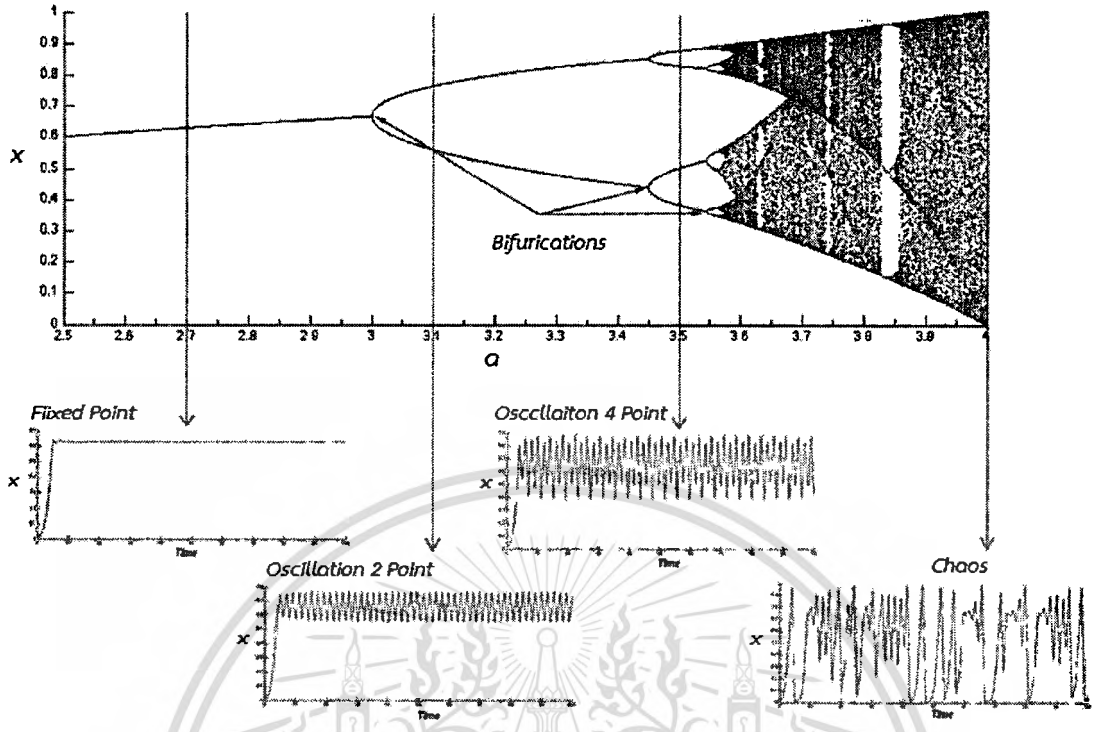


Fig. 3.2 A bifurcation diagram of Logistic map [53]

The bifurcation occurs when changing a parameter causes a dynamic system to "branch" into multiple values. In the case of logistic bifurcation, we are considering the limits or end behaviors of logistic systems. Recall that a logistic system is different from the Logistic map. The Logistic map only describes the end behavior between the current population size and the subsequent one and thus has no meaningful "end behavior." A logistic system, on the other hand, changes over time to approach either a steady value, a stable oscillation as shown in Figure 3.2, or a chaos.

The Feigenbaum constant ratio is the difference between the first bifurcation and the second bifurcation divided by that between the maximum and the first bifurcations, and it holds for all one-dimensional maps with a single quadratic maximum. As a consequence of this generality, every chaotic system that corresponds to this description will bifurcate at the same rate. The Feigenbaum constant [54] is given by:

$$\delta = \lim_{n\to\infty} \frac{a_{n-1} - a_{n-2}}{a_n - a_{n-1}} = 4.669201609102990671853203821\cdots \quad (3.7)$$

$$Ratio = \frac{a_{n-1} - a_{n-2}}{a_n - a_{n-1}} \tag{3.8}$$

where $a_n$ are discrete values of a at the *n*th period doubling.

As seen in Table 3.2, the ratio in the last column converges to the first Feigenbaum constant. The same number arises for the Logistic map with real parameter $a$ and variable $x$.

**Table 3.2** The Feigenbaum constant ratios of Logistic maps [54]

| *n* | *Period* | *Bifurcation parameter ($a_n$)* | *Ratio* |
|---|---|---|---|
| 1 | 2 | 3 | N/A |
| 2 | 4 | 3.4494897 | N/A |
| 3 | 8 | 3.5440903 | 4.7514 |
| 4 | 16 | 3.5644073 | 4.6562 |
| 5 | 32 | 3.5687594 | 4.6683 |
| 6 | 64 | 3.5696916 | 4.6686 |
| 7 | 128 | 3.5698913 | 4.6692 |
| 8 | 256 | 3.5699340 | 4.6692 |

The Logistic system, like many other dynamic systems, is created by applying a single process over and over to one initial condition. Therefore, any one step in a Logistic system, no matter how far it is from $x_0$, will look the same, mathematically, as any other single step. In this way, Logistic systems share an important characteristic with fractals, and visual representations of them often have fractal dimensions of self-similarity [55]. The Logistic bifurcation diagram is one such representation in which many parts of the diagram possess similar characteristics to the main diagram. As shown in Figure 3.3, the image on the right is a zoom-in image of a small section of the diagram of the left-hand image. The characteristics of the section appear similar to those of the main diagram.

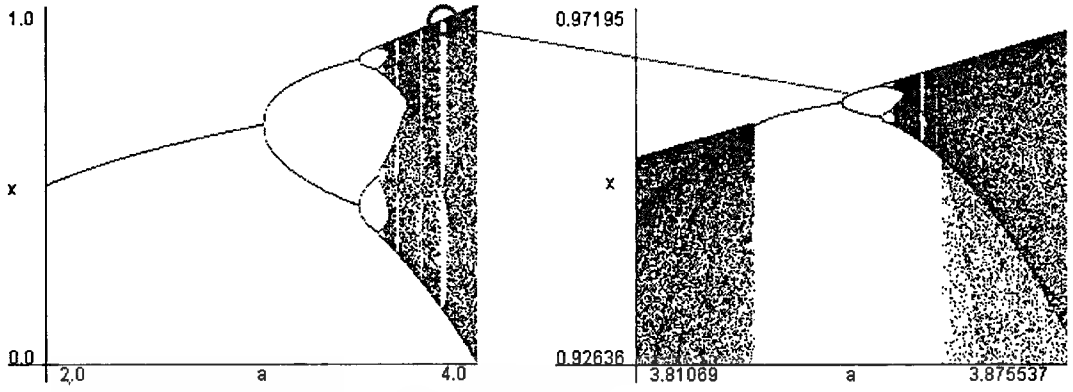


Fig. 3.3 The fractal properties of Logistic map [55]

## 3.4 Two-dimensional maps

Two-dimensional maps are corresponding to a particular set of differential equations, and they can be a representation of phase trajectory in a three dimensional maps. However, the two dimensional maps that are invertible, but show stretching and folding allowing positive Lyapunov exponents, are useful models for chaotic systems. Here we introduce four examples of two-dimensional maps discussed in various contexts [56].

- The Henon map

$$x_{n+1} = y_n + 1 - ax_n^2 \tag{3.9}$$
$$y_{n+1} = bx_n$$

- The Duffing map

$$x_{n+1} = y_n \tag{3.10}$$
$$y_{n+1} = -bx_n + ay_n - y_n^3$$

- The Kaplan-Yorke map

$$x_{n+1} = ax_n \bmod 1 \tag{3.11}$$
$$y_{n+1} = by_n + \cos(2\pi x_n)$$

- The Sinai map

$$x_{n+1} = (x + y + a\cos 2\pi y) \bmod 1 \tag{3.12}$$
$$y_{n+1} = (x + 2y) \bmod 1$$

The Hénon map is a discrete-time dynamical system. It is one of the most studied examples of dynamical systems that exhibit the chaotic behavior. The Hénon map takes a point $(x_n, y_n)$ in the plane and maps it to a new point. The map depends on two parameters, a and b, which for the classical Hénon map have values of $a = 1.4$ and $b = 0.3$. For the classical values, the Hénon map is chaotic. However, for other values of a and b, the map may be chaotic, intermittent, or converge to a periodic orbit. An overview of the type of behavior of the map at different parameter values may be obtained from its orbit diagram. The map was introduced by Michel Hénon as a simplified model of the Poincaré section of the Lorenz model. For the classical map, an initial point of the plane will either approach a set of points known as the Hénon strange attractor, or diverge to infinity.

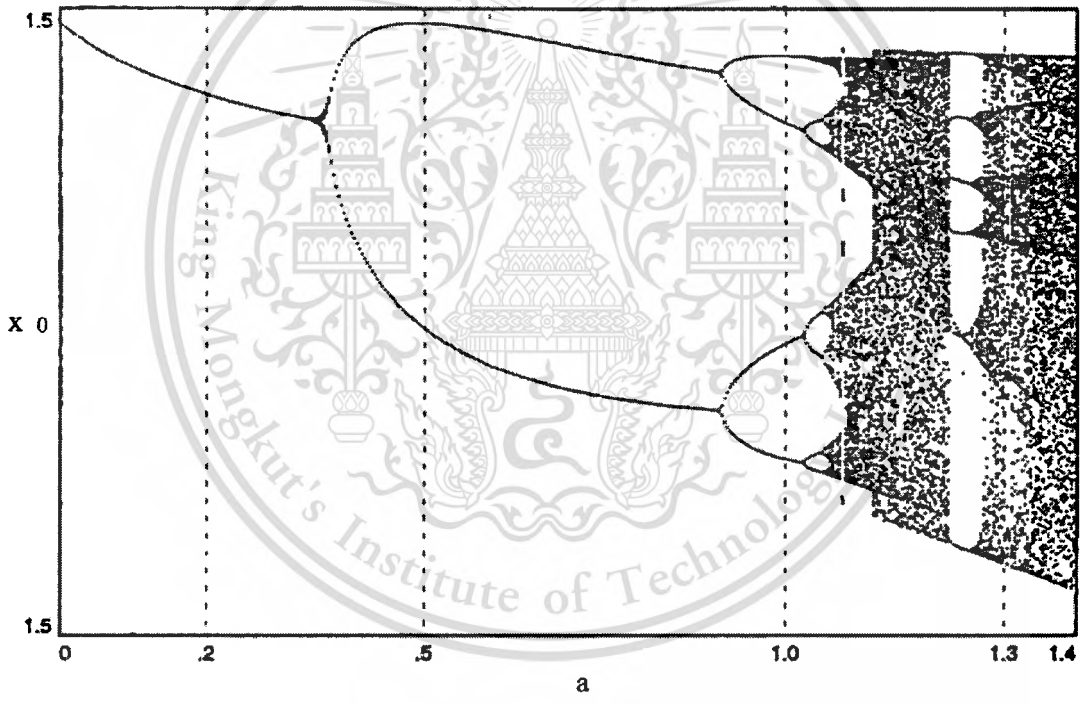


**Fig. 3.4** A Henon map bifurcation diagram [56]

## 3.5 Three-dimensional maps

Discrete chaotic systems, such as the Logistic map, can exhibit strange attractors irrespective of their dimensionality. In contrast, for continuous dynamical systems, a strange attractor can only arise in three or more dimensions. Finite

dimensional linear systems are never chaotic; for a dynamical system to display chaotic behavior, it has to be either nonlinear or infinite-dimensional.

The standard Lorenz attractor is generated by a system of three differential equations with a total of seven terms on the right hand side, five of which are linear terms and two of which are quadratic. Another well-known chaotic attractor is generated by the Rossler equations with seven terms on the right hand side, only one of which is nonlinear. Sprott discovered a three dimensional system with just five terms on the right hand side, and with just one quadratic nonlinearity which exhibits chaos for certain parameter values. The reason is that solutions to such systems are asymptotic to a two-dimensional surface and therefore are well behaved. A linear chaos theory is being developed in a branch of mathematical analysis known as functional analysis [57]. Below are examples of three dimensional chaotic equations.

The Lorenz attractor is defined by the system of following equations:

$$\begin{aligned} \frac{dx}{dt} &= a(y-x) \\ \frac{dy}{dt} &= cx - y - xz \\ \frac{dz}{dt} &= xy - bz \end{aligned} \tag{3.13}$$

The Chua attractor is defined by the system of following equations:

$$\begin{aligned} \frac{dx}{dt} &= a(y-x-f(x)) \\ \frac{dy}{dt} &= b(x-y+z) \\ \frac{dz}{dt} &= -cy \end{aligned} \tag{3.14}$$

where $f(x) = m_1 x + 0.5(m_0 - m_1)(|x+1| - |x-1|)$.

The Chen attractor is defined by the system of following equations:

$$\begin{aligned}\frac{dx}{dt} &= a(y-x)\\ \frac{dy}{dt} &= (c-a)x - xz + cy\\ \frac{dz}{dt} &= xy - bz\end{aligned} \tag{3.15}$$

The Rossler attractor is defined by the system of following equations:

$$\begin{aligned}\frac{dx}{dt} &= -y - z\\ \frac{dy}{dt} &= x - ay\\ \frac{dz}{dt} &= b + xz - cz\end{aligned} \tag{3.16}$$

The Sportt-Linz attractor is defined by the system of following equations:

$$\begin{aligned}\frac{dx}{dt} &= y\\ \frac{dy}{dt} &= -x + yz\\ \frac{dz}{dt} &= 1 - y^2\end{aligned} \tag{3.17}$$

The Arnold attractor is defined by the system of following equations:

$$\begin{aligned}\frac{dx}{dt} &= a\sin z + c\cos y\\ \frac{dy}{dt} &= b\sin x + a\cos z\\ \frac{dz}{dt} &= c\sin y + b\cos x\end{aligned} \tag{3.18}$$

These are some examples of chaotic equations in three-dimensional maps. Chaotic behaviors at the strange attractor can be generated by varying the initial condition and certain parameters in the chaotic equations.

## 3.6 Strange attractor

Chaotic behavior is of great interest when it occurs on an attractor since a large set of initial conditions will lead to orbits that converge to a chaotic region. An easy way to visualize a chaotic attractor is to start with a point in the basin of attraction of the attractor and then simply plot its subsequent orbit. Because of the topological transitivity condition, this is likely to produce a picture of the entire final attractor. Both orbits shown in Figure 3.5 give a picture of the general shape of the Lorenz attractor. This attractor results from a simple three-dimensional model of the Lorenz weather system. The Lorenz attractor is perhaps one of the best-known chaotic system diagrams probably because it is not only one of the first but also one of the most complex. Thus, this gives rise to a very interesting pattern which looks like the wings of a butterfly. Unlike fixed-point attractors and limit cycles, the attractors which arise from chaotic systems, known as strange attractors, have great details and complexity. Strange attractors occur in both continuous dynamical systems and certain discrete systems [58]. Figures 3.5-3.10 are examples of the strange attractors of three-dimensional equations with parameter values.

The Lorenz attractor with parameter values:

$$x_0, y_0, z_0 = [1,1,1] \text{ and } a, b, c = [10, 8/3, 28]$$

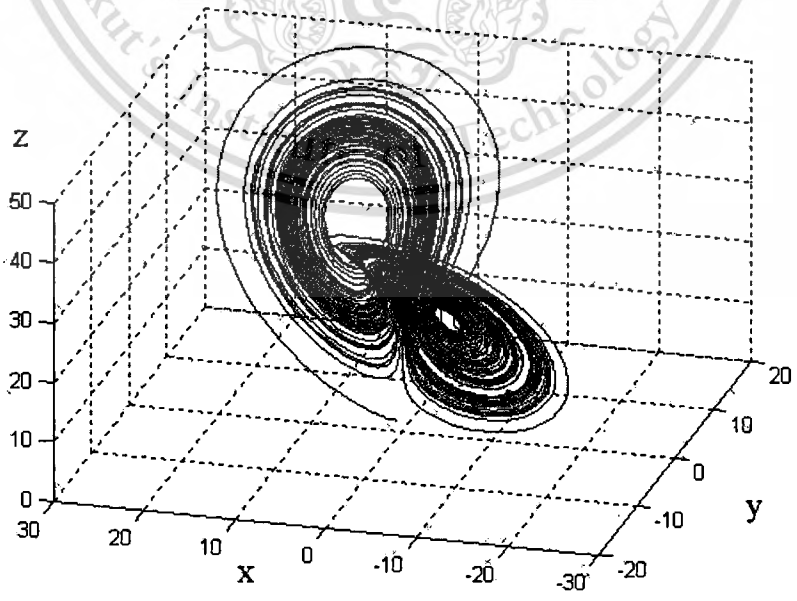


**Fig. 3.5** The Lorenz attractor

The Chua attractor with parameter values:

$x_0, y_0, z_0 = [0.1, 0.1, 0.1]$ and $a, b, c = [15.6, 1, 25.58]$ $m_0, m_1 = [-8/7, -5/7]$

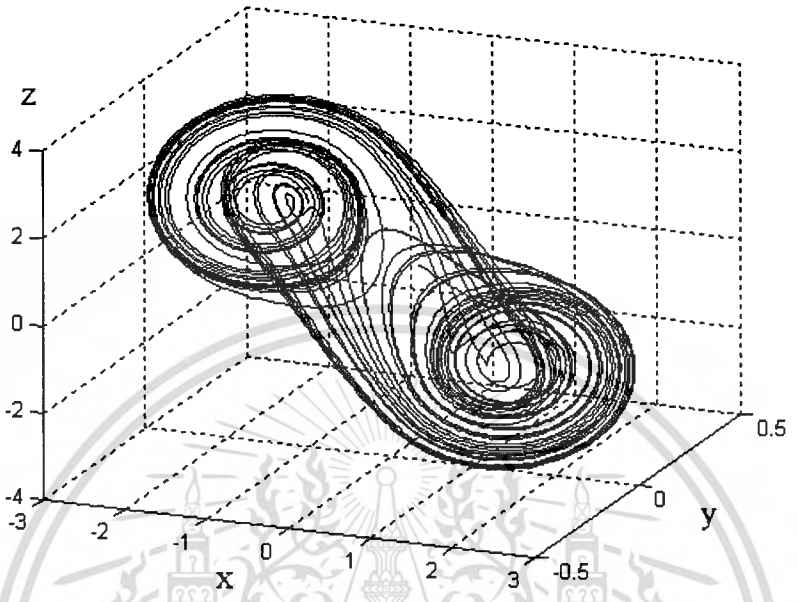


**Fig. 3.6** The Chua attractor

The Chen attractor with parameter values:

$x_0, y_0, z_0 = [-3, 2, 20]$ and $a, b, c = [35, 8/3, 28]$

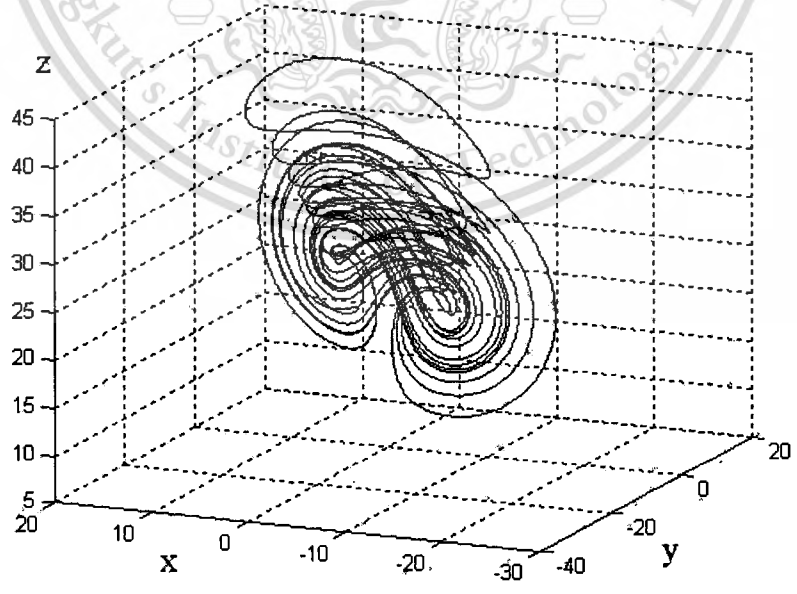


**Fig. 3.7** The Chen attractor

The Rossler attractor with parameter values:

$$x_0, y_0, z_0 = [1,1,1] \quad \text{and} \quad a, b, c = [0.2, 0.2, 5.7]$$

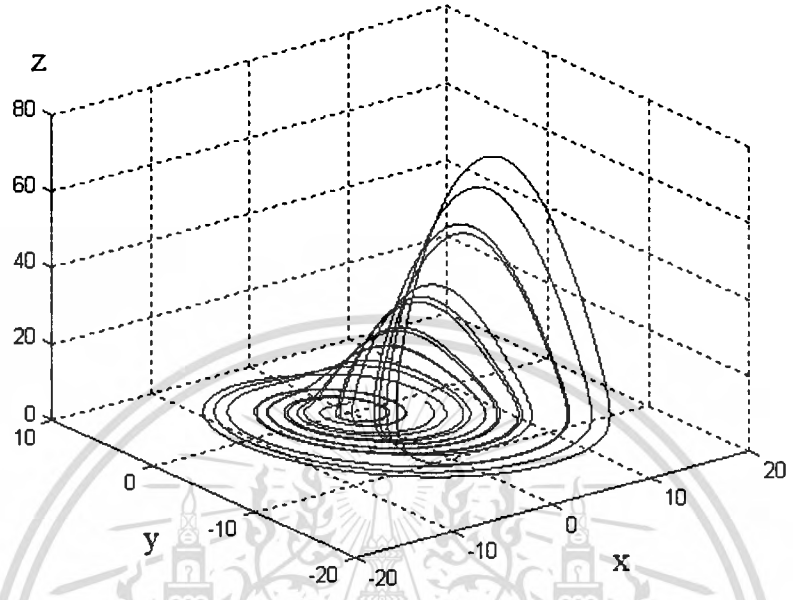


**Fig. 3.8** The Rossler attractor

The Sprott-Linz attractor with parameter values:

$$x_0, y_0, z_0 = [1,1,1]$$

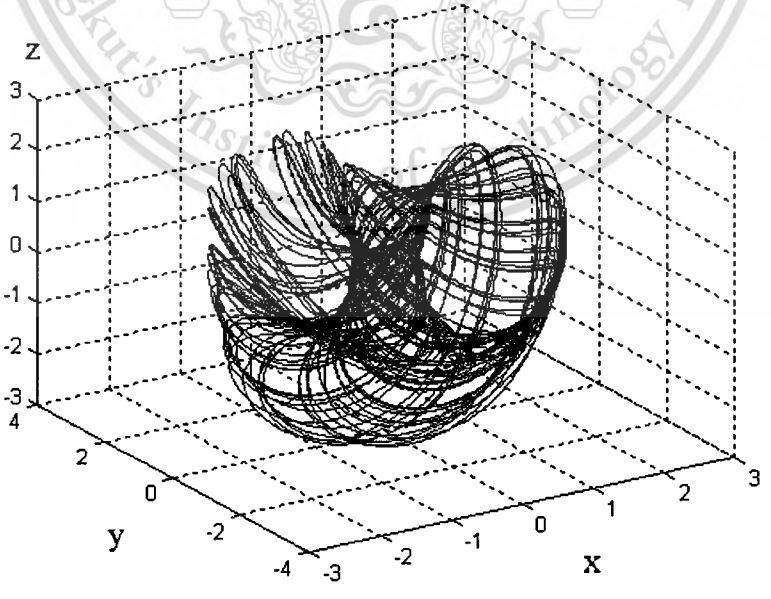


**Fig. 3.9** The Sprott-Linz attractor

The Arnold attractor with parameter values:

$$x_0, y_0, z_0 = [4,3.5,0] \text{and } a,b,c = [0.27,0.135,0.135]$$

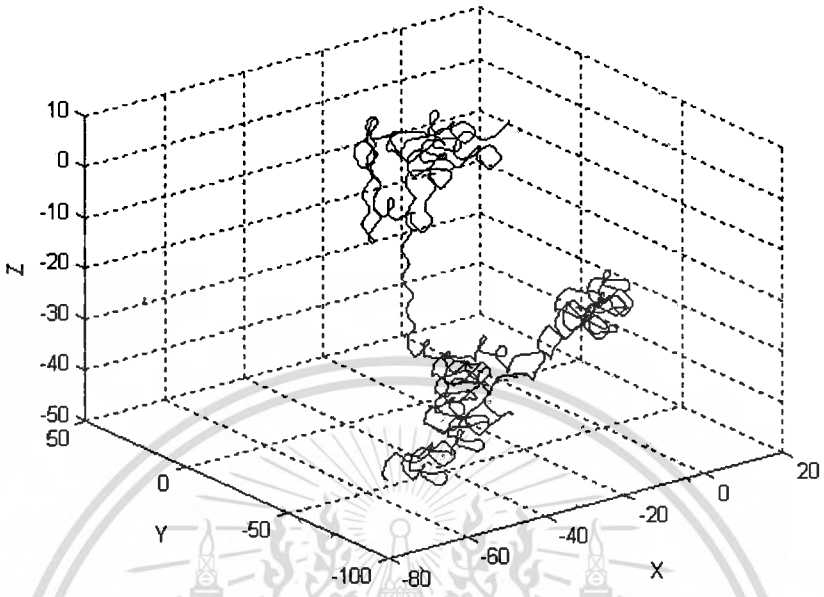


**Fig. 3.10** The Arnold attractor

## 3.7 Lyapunov exponents

The rate of separation can be different for different orientations of initial separation vector. Thus, there is a spectrum of Lyapunov exponents, which are equal in number to the dimensionality of the phase space. It is common to refer to the largest one as the Maximal Lyapunov exponent (MLE), because it contains a measure of predictability for a dynamical system. A positive MLE is usually taken as an indication that the system is chaotic (provided that some other conditions are met, e.g. phase space compactness). Note that an arbitrary initial separation vector typically contains some component in the direction associated with the MLE, and because of the exponential growth rate, the effect of the other exponents will be obliterated over time [59]. The Lyapunov exponent ($\lambda$) is useful for distinguishing various types of orbits and works for discrete and continuous systems. The Lyapunov exponent can be determined using the formula:

$$\lambda = \lim_{n\to\infty} \frac{1}{n} \sum_{i=0}^{n} \log_e \left| f'(x_i) \right| \tag{3.19}$$

**Table 3.3** The Lyapunov Exponents

| Dimension | Lyapunov exponent | | | Behavior |
|---|---|---|---|---|
| | $\lambda_1$ | $\lambda_2$ | $\lambda_3$ | |
| One-dimensional Map | - | | | Periodic Orbit |
| | 0 | | | Fixed Point |
| | + | | | Chaotic |
| Two-dimensional Map | - | - | | Fixed Point |
| | 0 | + | | Limit Cycle |
| | + | - | | Chaotic |
| Three-dimensional Map | - | - | - | Fixed Point |
| | 0 | - | - | Limit Cycle |
| | 0 | 0 | - | Quasi-Periodic Tours |
| | + | 0 | - | Chaotic |

The orbit attracts to a stable fixed point or stable periodic orbit at $\lambda<0$. Negative Lyapunov exponents are characteristic of dissipative or non-conservative systems (e.g. the damped harmonic oscillator). Such systems exhibit asymptotic

stability; the more negative the exponent, the greater the stability. Superstable fixed points and superstable periodic points have a Lyapunov exponent of $\lambda = -\infty$. This is something akin to a critically damped oscillator in that the system heads towards its equilibrium point as quickly as possible.

The orbit is a neutral fixed point at $\lambda = 0$. A Lyapunov exponent of zero indicates that the system is in relatively steady state mode. A physical system with this exponent is conservative. Such systems exhibit Lyapunov stability. Take the case of two identical simple harmonic oscillators with different amplitudes. Because the frequency is independent of the amplitude, a phase portrait of the two oscillators would be a pair of concentric circles. The orbits in this situation would maintain a constant separation, like two flecks of dust fixed in place on a rotating record.

The orbit is unstable and chaotic at $\lambda > 0$. Nearby points, no matter how close, diverge to any arbitrary separation. All neighborhoods in the phase space will eventually be visited. These points are unstable. For a discrete system, the orbits will look like snow on television screen (i.e. noise). This does not preclude any organization as a pattern may emerge. A physical example can be found in the Brownian motion. Although the system is deterministic, there is no order to the orbit that ensues.

### 3.8 Summary

This chapter discusses the chaotic phenomena and the basic equations of one-dimensional, two-dimensional and three-dimensional maps. The bifurcation examples of the Logistic and Henon maps are also presented. The Lyapunov exponents are employed to identify the chaotic systems of the one-dimensional, two-dimensional and three-dimensional maps. A positive Lyapunov exponent indicates the chaotic behavior of the map. The following chapter discusses the use of a tuning fork as a mechanical oscillator for classification of materials.

# Chapter 4

# Mechanical oscillator for sensing application

## 4.1 Introduction

This chapter is concerned with a mechanical oscillator for sensing application, while in Chapter 2 a tuning fork (TF) was provided as an example of the mechanical oscillator. A TF is a mechanical tool for generating an acoustic tone, whose structure is of U-shape and thus two prongs. It is possible to design the TF resonant frequency by varying the parameters, i.e. the prong length, the prong cross-section area, Young's modulus number elastic property, and material density. TFs have been reduced in size and have included a piezoelectric into the prongs since the late 1960s. The TF with piezoelectric (TFP) is in common use in the watch industry as it oscillates the clock frequency with high accuracy [62]. The main characteristics of TFP are its high amplitude output, high phase sensitivity, high quality factor ($Q$), small size, and robustness. Thus, the TFP can be found in a variety of applications, e.g. in level sensoring, in viscosity measurement, in liquid density measurement, and in the Pico-Newton force measurement [13].

A tuning fork with piezoelectric (TFP) is an electro-mechanical device whose principle is based on specific frequency and limited voltage. Theoretically, the TFP is a high sensitive device capable of detecting a tiny input signal. This dissertation presents a phase difference technique for material classification by which the phase difference can be determined from the difference between the input and output signals when the modified TFP is in contact with the material surface. The modified TFP is created by mounting a small needle on one end of the TFP prongs. The Bode's frequency response method is used to observe the modified TFP behavior and to select a specific frequency. The usefulness of the modified TFP has been reported in a number of research studies on the subject of nano-sensing. One specific application of the modified TPF is the surface sensing in the Atomic Force Microscopy (AFM) system in which an AFM image is generated by an interaction between a tungsten needle tip of the modified TFP and the material surface. The AFM imaging technique has been commonly employed for measurement of the biological micro-structure [20]. In addition, the technique can characterize the

magnetic properties of a hard-disk media surface in the submicron distance scale [16]. The AFM imaging technique utilizes the output signal amplitude and distance between the needle tip and the material to generate an AFM image. However, since the technique is unsuited for elastic materials, the phase difference technique is thus adopted to improve the AFM image quality [17].

To simulate the mechanisms of the modified TFP, there exist two models to use to carry out the simulation, i.e. the electrical and mechanical models. In the electrical model, a Butterworth-Van Dyke circuit, a simple resonance circuit, is used to perform the simulation [42]. The Butterworth-Van Dyke circuit synchronizes the TF resonance frequency of TF with that of piezoelectric (PZT). In the mechanical model, the sizes and dimensions of TF and PZT define the oscillation amplitude. Currently, a needle is typically manually mounted onto a TFP to obtain a modified TFP. Thus, the errors from manual installation can be expected to arise and thereby affect the TPF performance [18]. The errors are possibly caused by the needle mass, the glue mass and the adhesive position.

The experiment of this research work consists of two stages. The first stage is concerned with two needle mounting techniques: the shear-force mounting and the tapping mode mounting. Both mounting techniques are applied to the TFP prior to carrying out the tests. The test materials include hard plastic, metal, silicon rubber, vinyl eraser and hydrogel. The experimental results show that both mounting techniques are able to satisfactorily classify all the five test materials. Nevertheless, by comparison, the shear-force mounting technique performs better in classifying the test materials. In the second stage, the experiment is carried out only with silicon rubber as it is a highly elastic material, and the TFP with the shear-force mounting is selected due to a better performance. There are two sets of silicon rubber, i.e. normal silicon rubber and silicon rubber painted with an acrylic on the surface. The application of paint is to investigate whether the needle tip is able to classify the identical material with slightly different elasticity. The shear-force mounting TFP is mechanically shifted forward by 1 $\mu m$ per shift to allow for deeper penetration of the needle tip into the material surface. The amplitudes and phase data of all the test materials including the silicon rubber with acrylic are observed and documented. The technique used in the second stage is applicable to determining the condition of bio-cells in terms of the surface elastic properties.

## 4.2 Modeling

Figure 4.1 illustrates a TFP module, or a single-input-single-output (SISO) device, in which its input port is excited by a sinusoidal signal at various frequencies while simultaneously the TFP responses can be measured at the output port. In order to obtain the specific frequency of the TFP, the mechanical model and the electrical model are typically used.

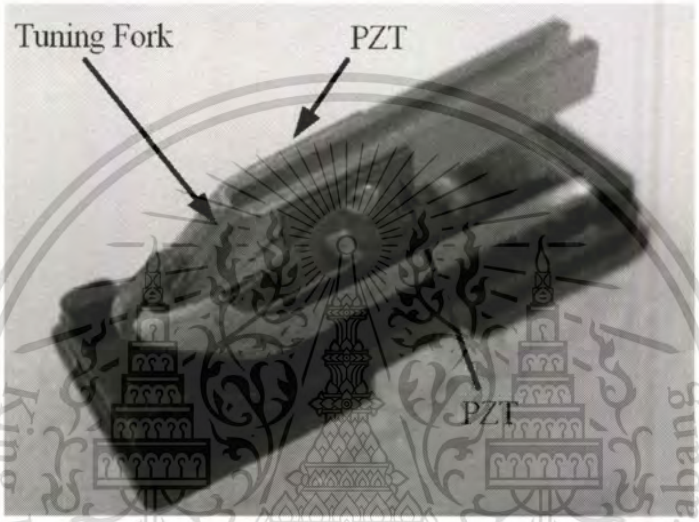


**Fig 4.1** A basic tuning fork with piezoelectric

In this dissertation the Bode's frequency response method is employed and its results are subsequently used to approximate the TFP mathematical model. The first-order model with cascade notch filters is applied to damp the resonances. According to [63, 64], the TF can be described as:

$$TF_1 = \frac{\omega_l}{\varpi + \omega_l} \tag{4.1}$$

$$TF_2 = \prod_{i=1}^{j} \frac{s^2 + 2\zeta_{1i}\omega_i s + \omega_i^2}{s^2 + 2\zeta_{2i}\omega_i s + \omega_i^2} \tag{4.2}$$

where $\omega_l$ is a low-pass frequency (rad/sec), $\tau$ is a time delay of tuning fork (sec), $\omega_i$ is a resonance frequency (rad/sec), $\xi_{1i}$ and $\xi_{2i}$ are damping ratios selected to notch

resonance peak, $i$ is an index number of resonance frequency, and $j$ is a last number of resonance frequency. We can achieve the TFP transfer function as follows:

$$TF_{TFP} = \frac{\omega_l}{s + \omega_l} \times \prod_{i=1}^{j} \frac{s^2 + 2\zeta_{1i}\omega_i s + \omega_i^2}{s^2 + 2\zeta_{2i}\omega_i s + \omega_i^2} \tag{4.3}$$

Figure 4.2(a) depicts the TFP Bode's plot with the test frequencies gradually rising from 100 Hz to 18 kHz. The simulation of the TFP model is carried out after obtaining the gains and the phase plots, and the simulation result is presented in Figure 4.2(b). From Eq. (4.3), the TFP mathematical model can be derived as (Eq.4.4):

$$TF_{TFP} = \frac{628}{0.06s + 628} \times \frac{s^2 - 37s + 355305758}{s^2 - 10s + 355305758} \times \frac{s^2 + 131.946s + 4352495540}{s^2 + 45s + 4352495540} \times \frac{s^2 + 165.042s + 6809793154}{s^2 + 25s + 6809793154} \times \frac{s^2 + 212.748s + 11315497498}{s^2 + 14s + 11315497498} \tag{4.4}$$

In Eq.(4.3), $\omega_1$, $\omega_2$, $\omega_3$ and $\omega_4$ are 18,849.55 rad/sec (3kHz), 65,973.445 rad/sec (10.5 kHz), 82,521.471 rad/sec (13.1337 kHz) and 106,374.327 rad/sec (16.930 kHz), respectively. As $\xi_{1i}$ are close to natural resonance damping, they are fixed at 0.001. Meanwhile, $\xi_{2i}$ are adjustable using the signal gain (dB).

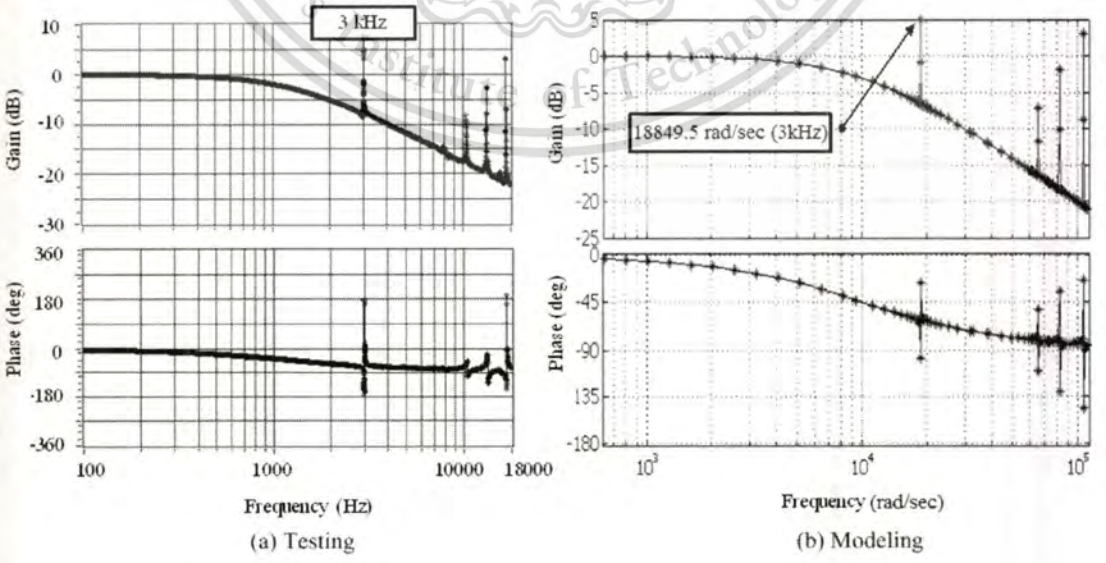


**Fig 4.2** The frequency response of the basic TFP device: (a) Testing, (b) Modeling

## 4.3. Modified TFP

In a modified TFP in which a needle is mounted onto a standard TFP, the tip of the needle is of paramount importance as it is the part that is in direct contact with the materials. The needle is of tungsten and its tip is reduced in size by the electrochemical polishing method. The needle dimensions are 4 mm long and 0.4 mm across with the width of the needle tip of 0.1 mm, as shown in Figure 4.3. Two types of mounting are adopted to mount the needle on to the TFP: the shear-force mounting and the tapping mode mounting. The perspective views of the shear-force mounting and the tapping mode mounting are respectively illustrated in Figures 4.4a-b. Figures 4.5a-b depict the degrees of the needle mounting for the shear-force and the tapping mode, respectively. After the completion of the modifications and thereby the modified TFPs, the frequency response tests are carried out to examine the dissimilarities between the basic TFP and the two modified TFPs. Figure 4.7 shows the frequency responses.

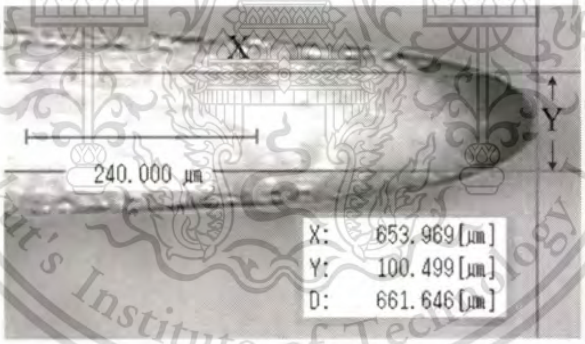


**Fig 4.3.** The dimensions of the needle and its tip.

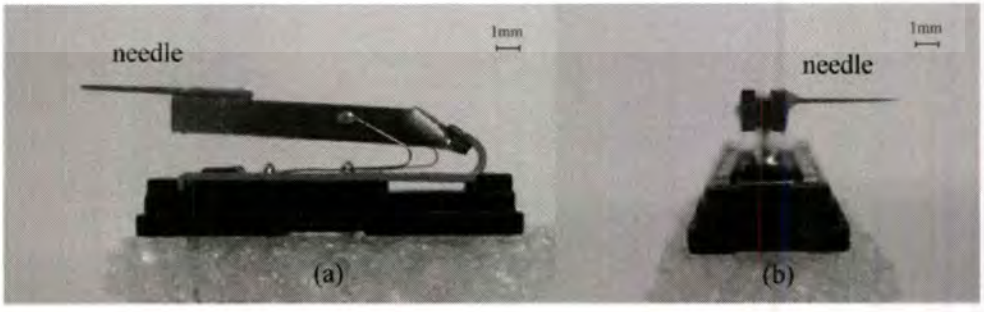


**Fig 4.4** The perspective views of (a) the shear-force mounting and (b) the tapping mode mounting of the needle.

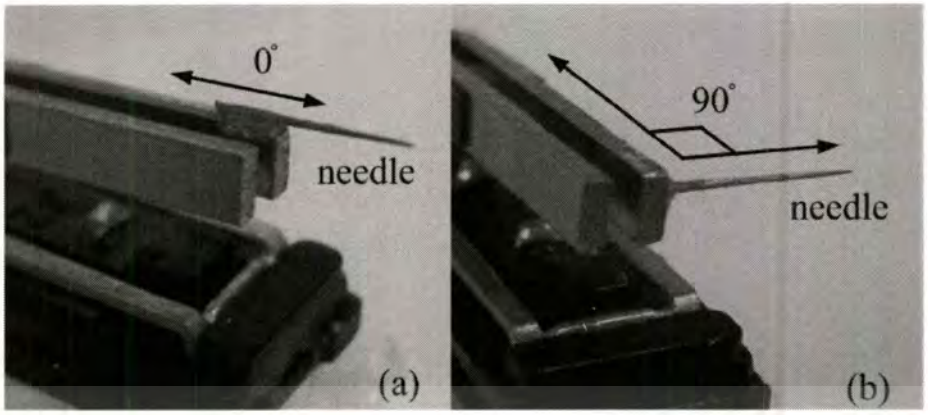


**Fig 4.5** The degrees of needle mounting in (a) the shear-force mounting and (b) the tapping mode mounting.

As shown in Figure 4.6, the 3 Vp-p function generator generates the sine wave signals and sweeps the frequency from 100Hz to 18 kHz. The sine wave signals of various frequencies are transmitted to PZT1 and then to PZT2 of the tuning fork with a needle mounted. The measurement of amplitudes and phases is performed at PZT2, as shown in Figure 4.7. It is found that the mounting location of the needle on the tuning fork and the needle mass affect the frequency response. The farther the distance of the needle location from the fork end, the more distorted the frequency response; and the more the needle mass, the greater the distortion. In addition, the manual mounting of the needle affects the frequency response; however, this issue can be effectively tackled with an adjustment of the tuning fork capacitor [19]. The adjustment is made through the basic electronic elements to increase the quality factor, thereby minimizing the error.

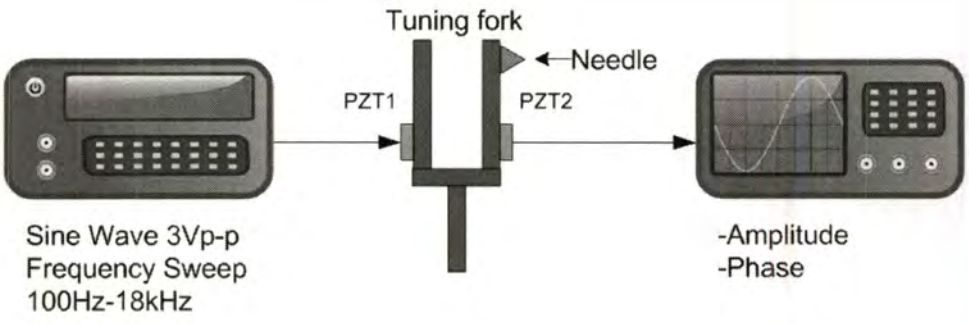


**Fig 4.6** Measurement process of frequency response of modified TFP

The frequency responses indicate that the resonance frequencies of the TFPs are slightly altered due to the needle. In the case of the shear-force mounting, as shown in Figure 4.7(a) the resonance reduces from 3 kHz to 2.935 kHz, while in the tapping mode mounting case, the resonance decreases from 3 kHz to 2.924 kHz, as shown in Figure 4.7(b).

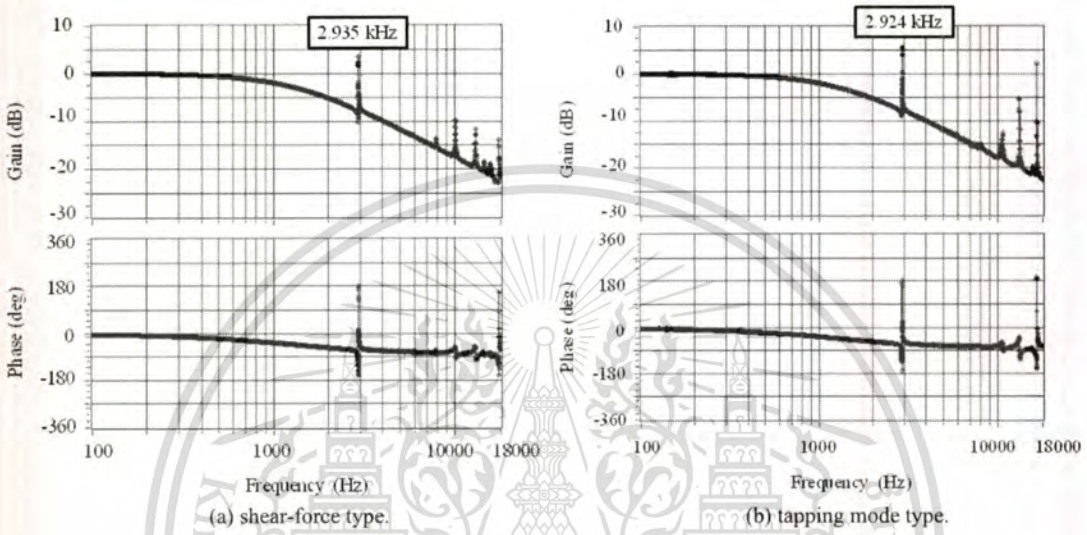


**Fig 4.7** The frequency responses of the modified TFPs: (a) shear-force mounting, (b) tapping mode mounting

## 4.4 Experiments

The experiments aim to examine and compare the performances of two types of modified TFPs, i.e. the shear-force mounting and tapping mode mounting TFPs. Three testing formats are used in the experiments: the stationary xy-plane with vertical moving z-plane; the moving xyz-plane; and the stationary xy-plane with chaotic motion z-plane (i.e. the chaotic motion z-plane). In the stationary xy-plane with vertical moving z-plane, hard plastic, metal, silicon rubber, vinyl eraser and hydrogel are used as the test materials. In the moving xyz-plane testing format, the test materials consist of only normal silicon rubber and silicon rubber painted with an acrylic. In the case of the chaotic motion z-plane, the chaotic motion is assumed to simulate the motions of living cells.

### 4.4.1 The stationary xy-plane with vertical moving z-plane

The tests are performed with hard plastic, metal, silicon rubber, vinyl eraser and hydrogel. Figure 4.9 is the photograph of the apparatuses used in the experiments in the stationary xy-plane with vertical moving z-plane case, i.e. a personal computer, a one-axis stand and a National Instrument (NI) controller of myDAQ model with 2 analog in/out ports and 8 digital in/out ports to generate 3Vp-p sine waves and receive the modified TFP output signals.

The frequencies of 2.935 and 2.924 kHz from the frequency response tests are utilized with the shear-force mounting and tapping mode mounting TFPs, respectively, to classify the test materials. The selected frequencies are proved to be able to effectively excite the modified TFPs. In the stationary xy-plane with vertical moving z-plane case, classification of the test materials involves two steps: (1) equate the input-output voltages (i.e. 3 Vp-p) by applying more force to the needle to penetrate deeper into the test material surface until both voltages are equal; and (2) determine the phase differences between the input and output signals. The time series plots of phase differences of the test materials are depicted in Figures 4.10-4.13, while Tables 4.1-4.4 present the shifted phases.

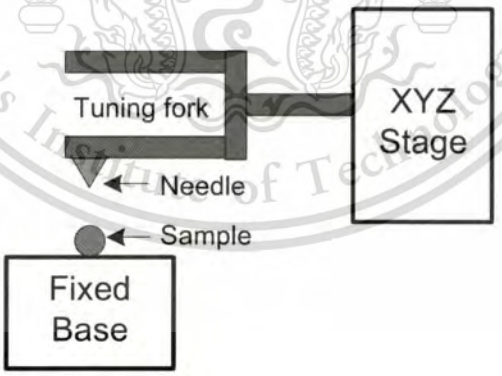


**Fig 4.8** The stationary xy-plane with vertical moving z-plane in which the test material (sample) is stationary and the needle moves vertically

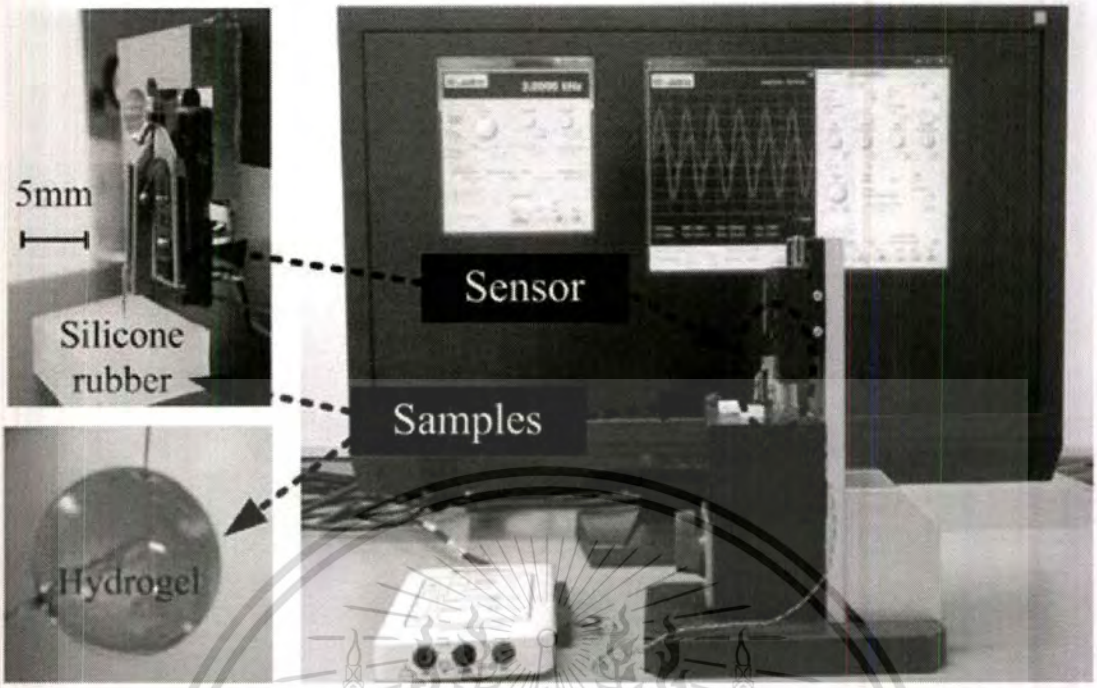


**Fig 4.9** A photograph of the apparatuses and test materials used in the stationary xy-plane with vertical moving z-plane testing

As shown in Figures 4.8 - 4.9, needle proximity to the test material (sample) is varied by the XYZ-stage device. The test materials are hard plastic, metal, silicon rubber, vinyl eraser and hydrogel. Hard plastic and metal are collectively called "hard materials". When the needle tip contacts the sample, the amplitude of output signal at PZT2 decreases.

As shown in Figure 4.10, the output signal drops in an uncontrollable manner when the needle tip is in contact with the hard materials, i.e. hard plastic and metal. Therefore, the phase difference tests are not carried out with hard plastic and metal.

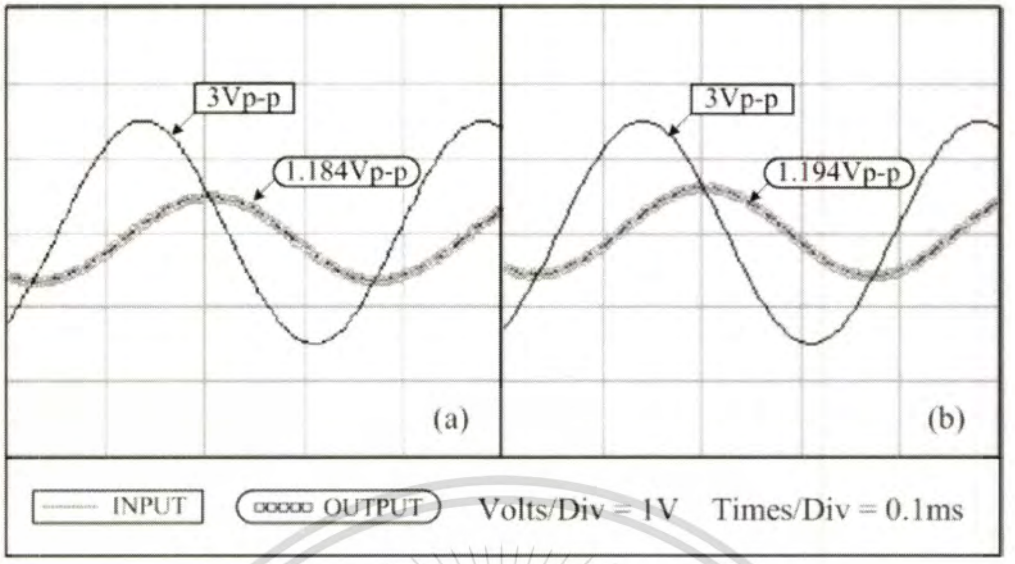


**Fig 4.10** The input and output signals of hard materials: (a) the shear-force mounting and (b) the tapping mode mounting.

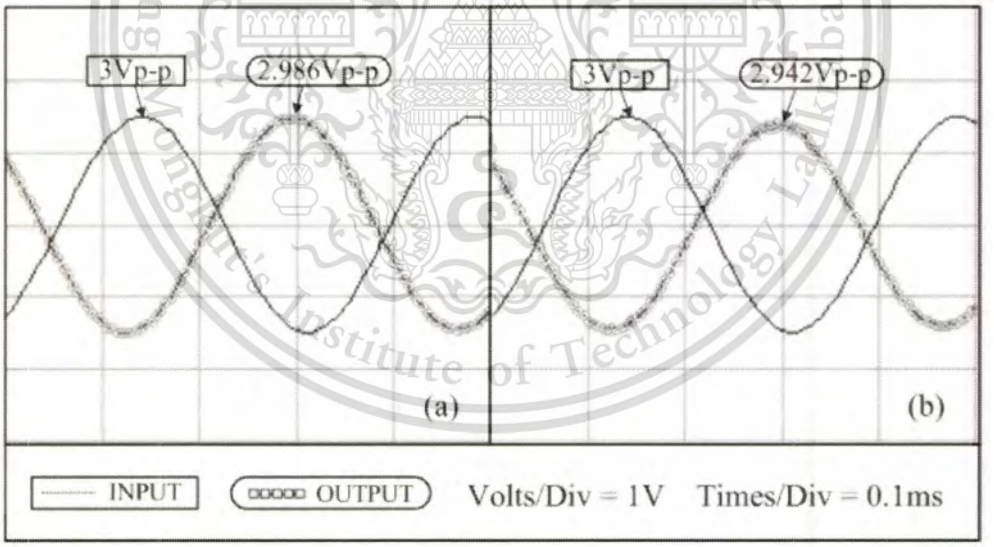


**Fig 4.11** The input and output signals of silicon rubber: (a) the shear-force mounting and (b) the tapping mode mounting.

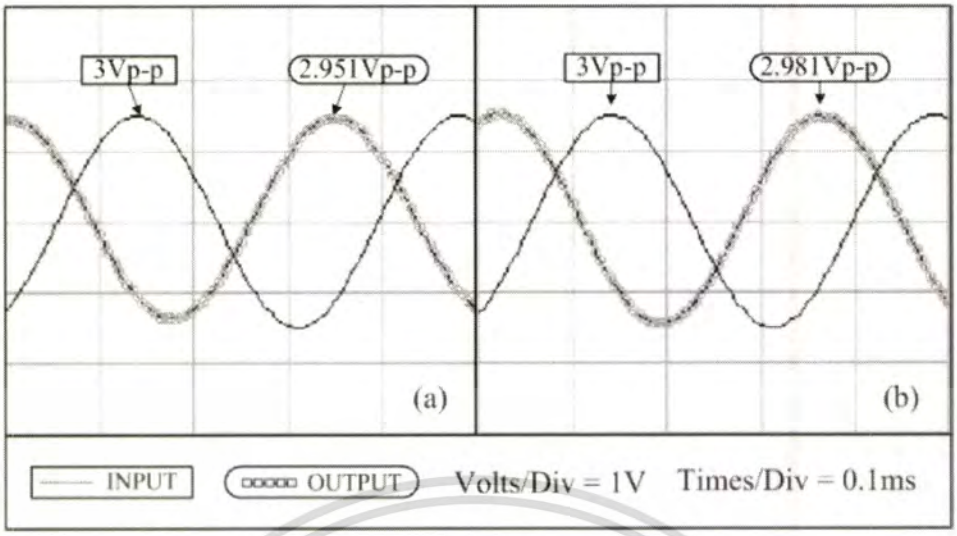


**Fig 4.12** The input and output signals of vinyl eraser: (a) the shear-force mounting and (b) the tapping mode mounting.

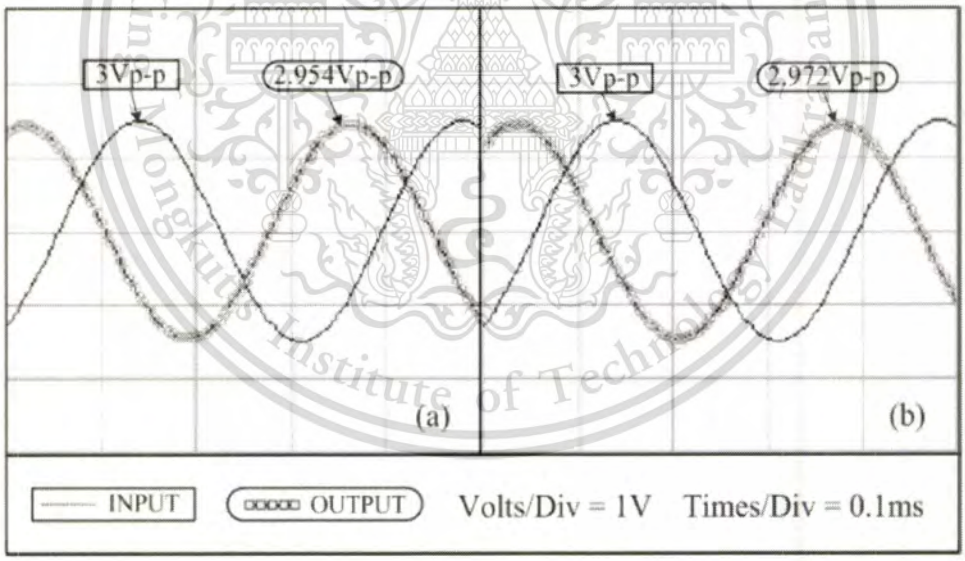


**Fig 4.13** The input and output signals of hydrogel: (a) the shear-force mounting and (b) the tapping mode mounting.

Figures 4.11-4.13 illustrate the input and output signals from the experiments, and it is possible to determine the phase difference values based on these signals. The signals achieved with the shear-force mounting type are presented in the

rectangular box (a), while the signals obtained with the tapping mode mounting type are in the box (b). As previously mentioned, the phase difference tests are not performed for hard plastic and metal due to uncontrollable drop of output signals. Tables 4.1-4.4 present the shifted phases of silicone rubber, vinyl eraser and hydrogel tested with the shear-force mounting and the tapping mode mounting TFPs. The tests are repeated 5 times for each test material.

**Table 4.1** The shifted phases tested with the shear-force mounting TFP

| Material | 1 | 2 | 3 | 4 | 5 | Average |
|---|---|---|---|---|---|---|
| Silicone rubber | -156.72 | -156.96 | -156.20 | -156.64 | -155.98 | -156.50 |
| Vinyl eraser | -216.35 | -216.59 | -216.77 | -216.92 | -216.24 | -216.57 |
| Hydrogel | -232.25 | -233.14 | -232.98 | -232.61 | -232.29 | -232.65 |

**Table 4.2** The shifted phases tested with the tapping mode mounting TFP

| Material | 1 | 2 | 3 | 4 | 5 | Average |
|---|---|---|---|---|---|---|
| Silicone rubber | -157.78 | -157.67 | -157.92 | -157.29 | -157.10 | -157.55 |
| Vinyl eraser | -222.23 | -221.67 | -221.49 | -221.22 | -221.58 | -221.64 |
| Hydrogel | -253.95 | -253.74 | -253.83 | -253.69 | -253.78 | -253.80 |

**Table 4.3** The shifted phases tested with the shear-force mounting TFP with $Q$ factor and phase adjustment added

| Material | 1 | 2 | 3 | 4 | 5 | Average |
|---|---|---|---|---|---|---|
| Silicone rubber | -134.91 | -134.93 | -135.92 | -135.63 | -136.11 | -135.50 |
| Vinyl eraser | -198.42 | -198.67 | -198.80 | -198.52 | -198.17 | -198.52 |
| Hydrogel | -230.34 | -230.87 | -231.12 | -230.65 | -231.49 | -230.89 |

**Table 4.4** The shifted phases tested with the tapping mode mounting TFP with $Q$ factor and phase adjustment added

| Material | 1 | 2 | 3 | 4 | 5 | Average |
|---|---|---|---|---|---|---|
| Silicone rubber | -136.42 | -136.56 | -136.32 | -136.76 | -136.12 | -136.44 |
| Vinyl eraser | -200.87 | -200.34 | -200.65 | -199.85 | -200.32 | -200.41 |
| Hydrogel | -232.21 | -231.52 | -231.66 | -231.98 | -231.60 | -231.79 |

Tables 4.1-4.2 present the shifted phases of silicone rubber, vinyl eraser and hydrogel tested with the shear-force and tapping mode mounting TFPs without $Q$ factor and phase adjustment, whereas Tables 4.3-4.4 present those with $Q$ factor and phase adjustment.

### 4.4.2 The moving xyz-plane testing

As shown in Figure 4.14, the XYZ-stage device regulates the movement of the TPF. The Z-stage device is moveable in the range of 1-10 $\mu m$ with 1 $\mu m$ per move. A displacement sensor measures the z-plane movement of the test materials and sends analog voltage to the position controller, which in turn regulates the movements of XYZ-stage and Z-stage devices. The moving xyz-plane tests are carried out with only elastic normal silicone rubber and silicone rubber spray-painted with acrylic as it is speculated that different surface elasticities of an identical material could influence the classification capability of TPFs.

Figure 4.15 shows the apparatuses of the moving xyz-plane testing using the displacement sensor and the position controller. The depth of the needle tip into the sample surface is increased by an increment of 1 $\mu m$ from 1 to 10 $\mu m$. The ratios of phase difference and amplitude of silicon rubber and silicon rubber with acrylic are illustrated Figures 4.16 and 4.17. By comparison, the difference of phase difference ratios of silicon rubber and silicon rubber with acrylic is greater than that of amplitude ratios of the same materials. Hence, the phase difference is better at classification of test materials.

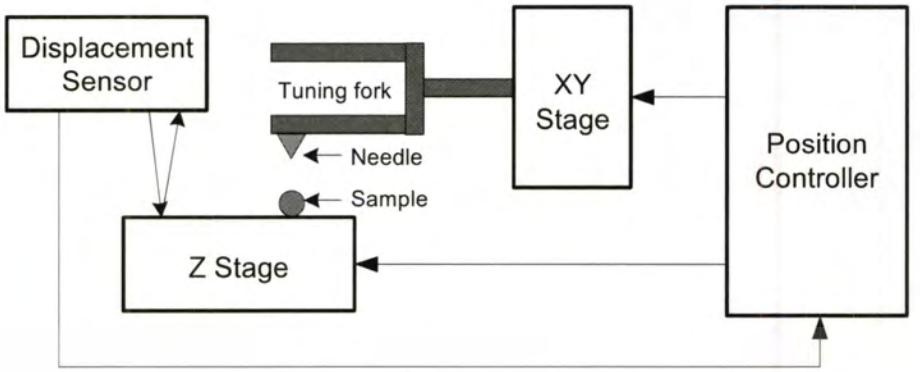


**Fig 4.14** The moving xyz-plane testing using a displacement sensor and a position controller.

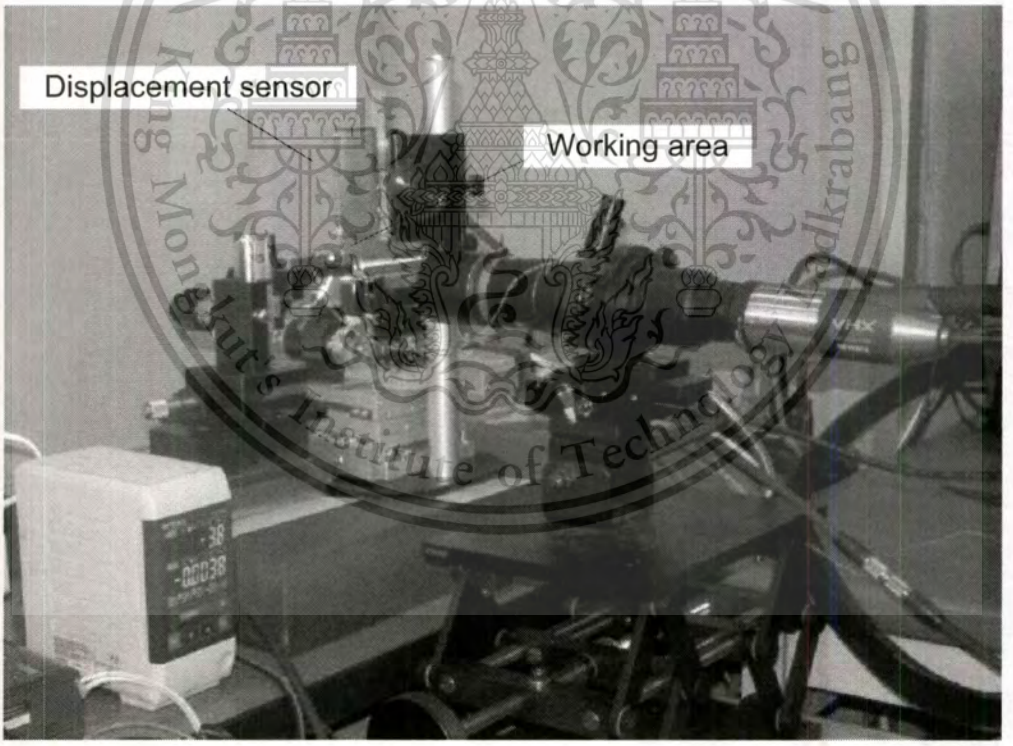


**Fig 4.15** A photograph of the apparatuses of the moving xyz-plane testing using a displacement sensor and a position controller.

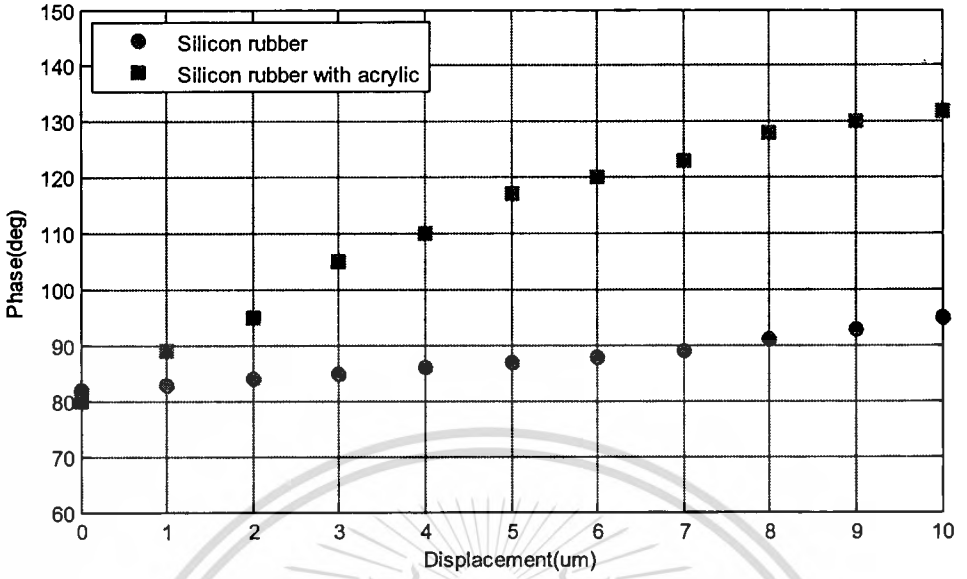


**Fig 4.16** The ratios of phase differences of silicon rubber and silicon rubber with acrylic

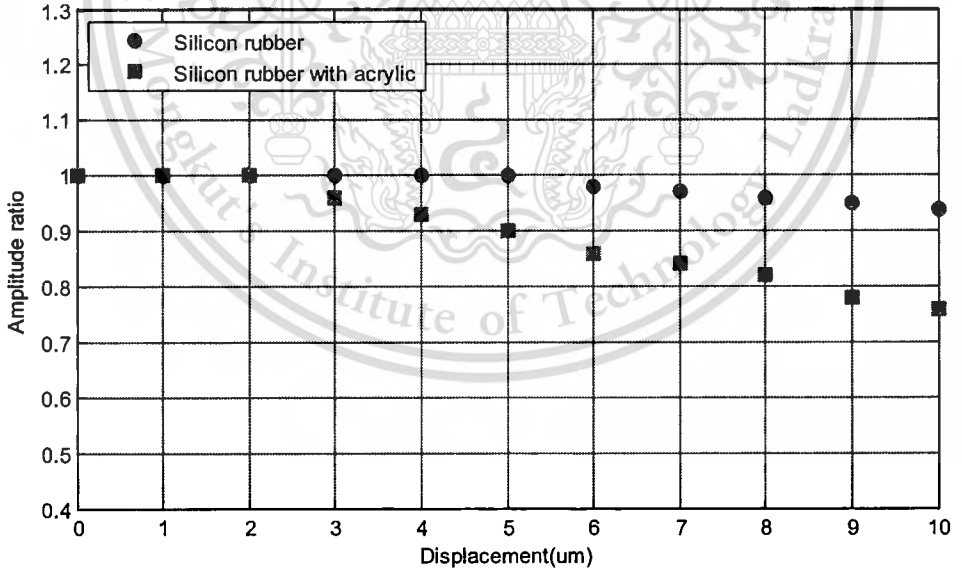


**Fig 4.17** The amplitude ratios of silicon rubber and silicon rubber with acrylic

### 4.4.3 The chaotic motion z-plane

This experiment uses the chaotic motion to simulate the living cells. The chaotic motion is generated by the simple logistic map equation discussed in Chapter 3. Figures 4.18-4.20 illustrates examples of chaotic motion generated with the equation. The phase differences of z-plane are measured. In the chaotic motion testing, only silicon rubber with acrylic is used as test material. Figures 4.21, 4.23 and 4.25 show the displacement versus phase response, while Figures 4.22, 4.24 and 4.26 display the normalized output ratio of chaotic motion.

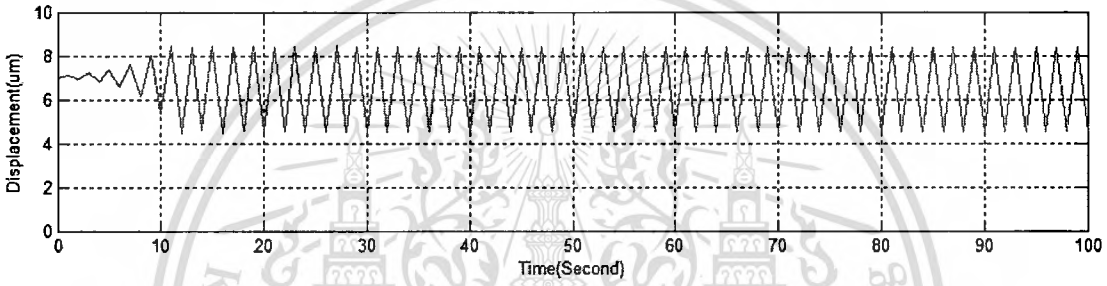


**Fig 4.18** The period motion (logistic a=3.4)

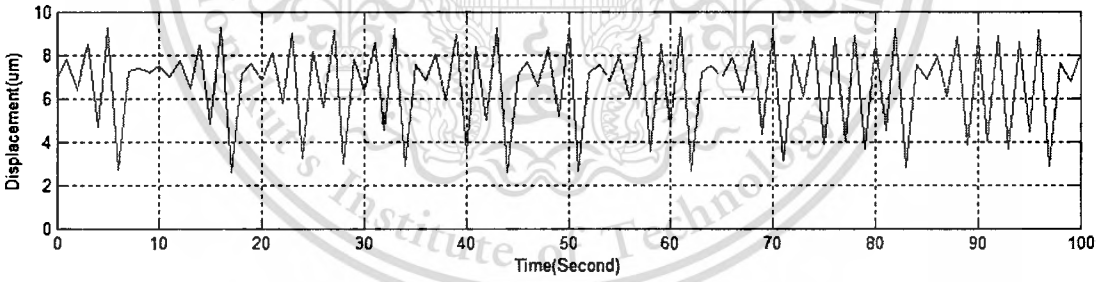


**Fig 4.19** The low chaotic motion (logistic a=3.7)

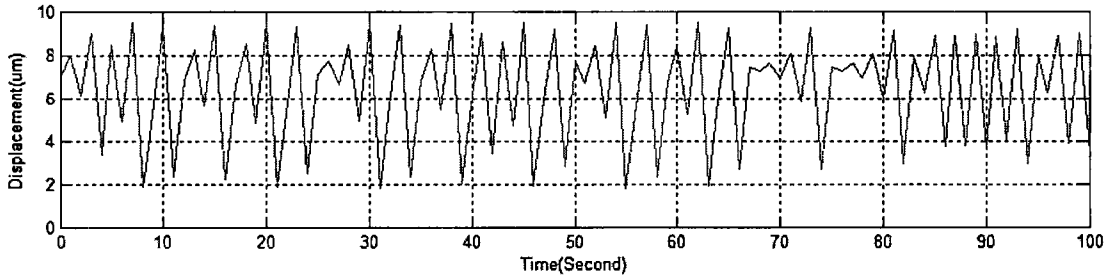


**Fig 4.20** The high chaotic motion (logistic a=3.8)

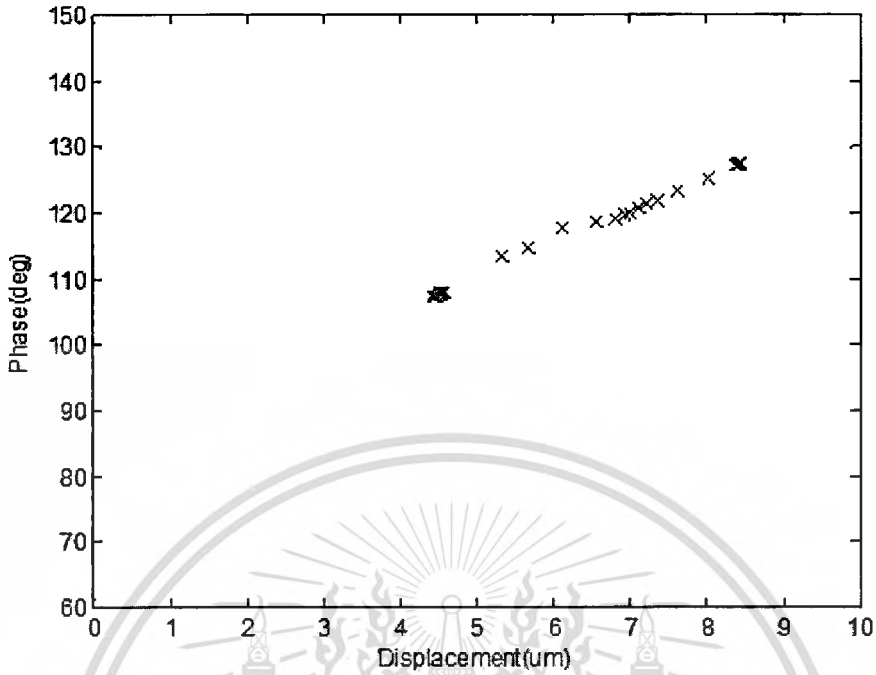


**Fig 4.21** The displacement versus phase response of period motion (logistic a=3.4)

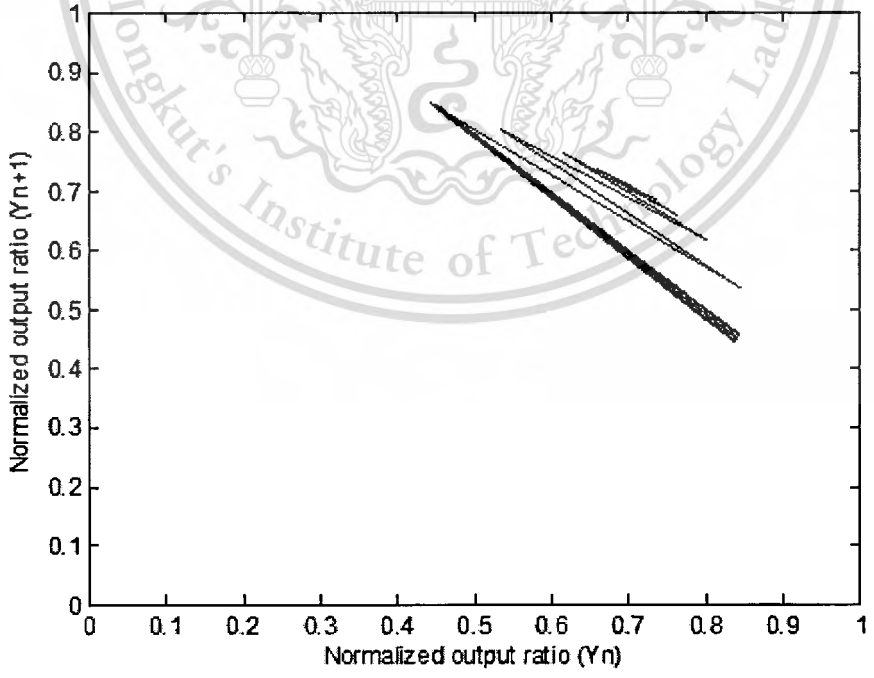


**Fig 4.22** The normalized output ratio of period motion (logistic a=3.4)

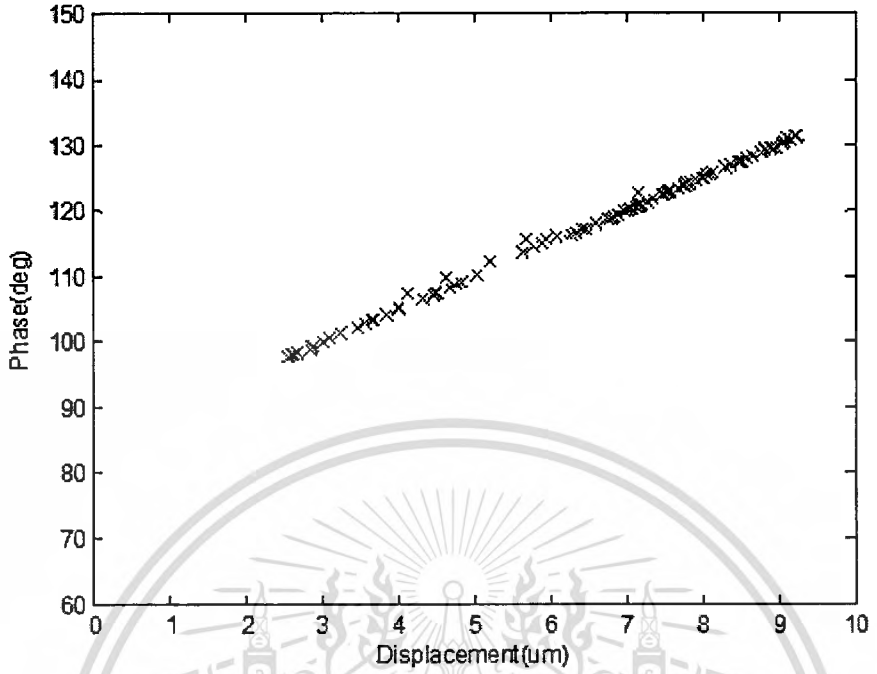


**Fig 4.23** The displacement versus phase response of low chaotic motion (logistic a=3.7)

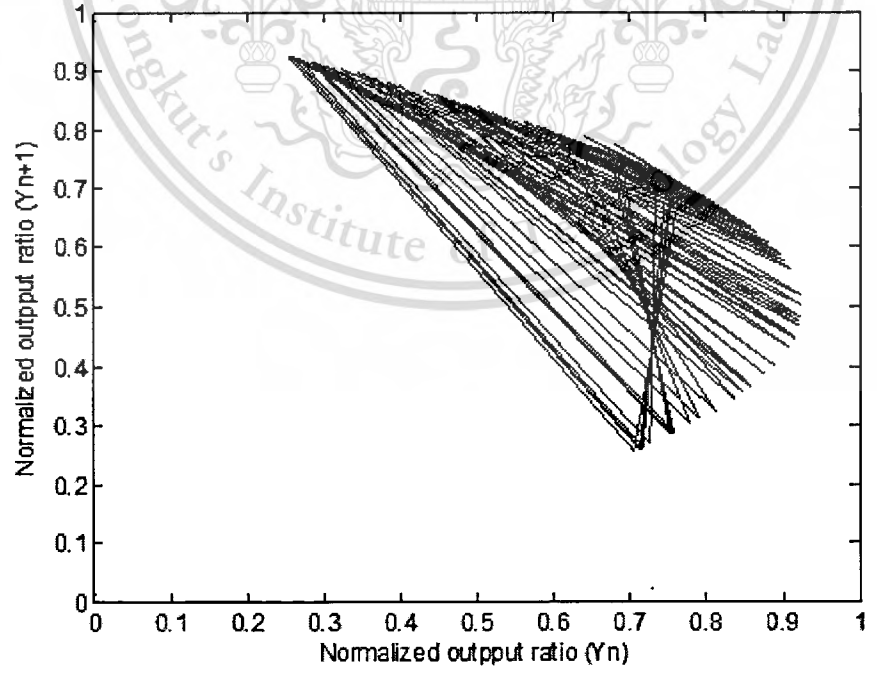


**Fig 4.24** The normalized output ratio of low chaotic motion (logistic a=3.7)

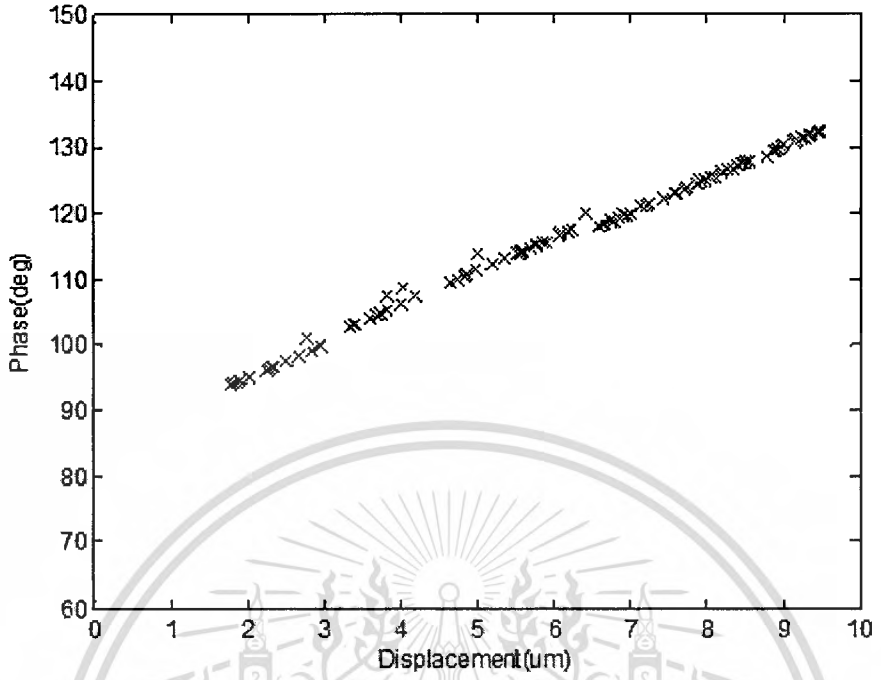


**Fig 4.25** The displacement versus phase response of high chaotic motion (logistic a=3.8)

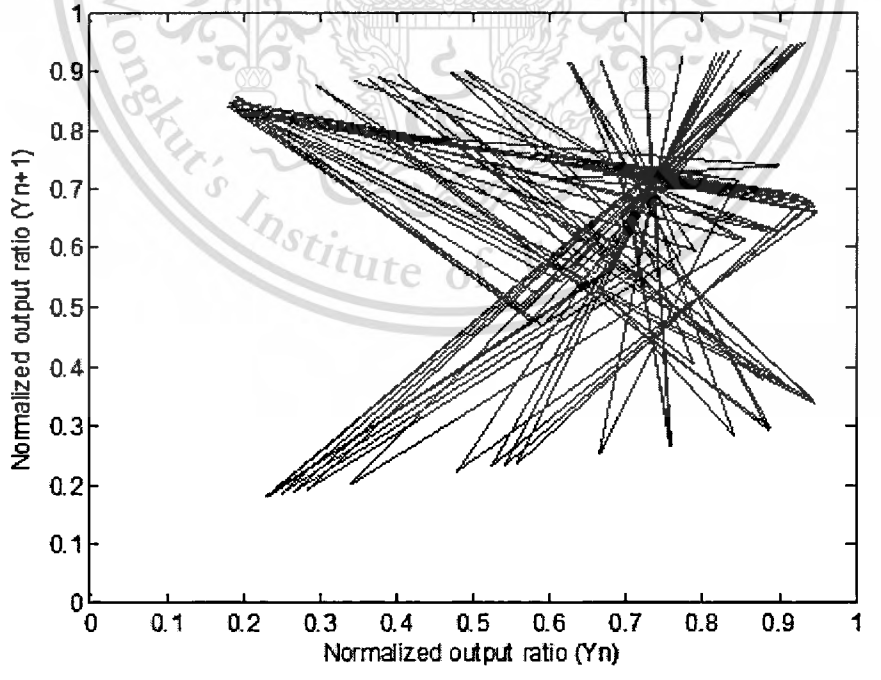


**Fig 4.26** The normalized output ratio of high chaotic motion (logistic a=3.8)

## 4.5 Summary

The Bode's frequency response method can be applied to study frequency domain behaviors and approximate a mathematical model for a modified TFP. The method is a commonly used electrical engineering tool to select a proper frequency. This research proposes the material classification method using phase differences and discusses two types of modified TFP, i.e. shear-force and tapping mode mounting TFPs. The phase differences are obtained by touching the needle tips of the modified TFPs on test materials. Except for hard plastic and metal, silicon rubber, vinyl eraser and hydrogel can be readily identified by moving the needle tip deeper into the surface of the materials until the input and output voltages are identical. The proposed phase difference technique is suitable for classification of elastomer materials. The performances of the proposed technique are presented in time series plots. The results of chaotic motion testing are presented in normalized output ratios. Chapter 5 is concerned with the application of chaotic motion in industrial microwave heating.

# Chapter 5

# Chaotic application for industrial microwave heating

## 5.1 Introduction

In most industrial applications, the mechanical movement of parts and components is common and thereby unnecessarily contributes to energy wastage. In addition, a long continuous movement can bring about wear and tear. Thus, a reduction in the unnecessary mechanical movement of the components of machinery and devices would lower the energy and maintenance costs. At present, there are many possible applications of the chaotic motion in both industrial equipment and household appliances. In the industrial applications, the concept of chaotic motion has been applied to, for example, mixers, grinders and compactors; and in the household appliances, it is applied to, for instance, dishwashers, washing machines, heaters, ventilating fans and vacuum cleaners, with the aim to improve the motion performance of the machinery and appliances. This chapter is concerned with a novel application of the chaotic motion to carbonization in a carbonization plant that adopts the non-stirring multi-feed microwave heating system [60].

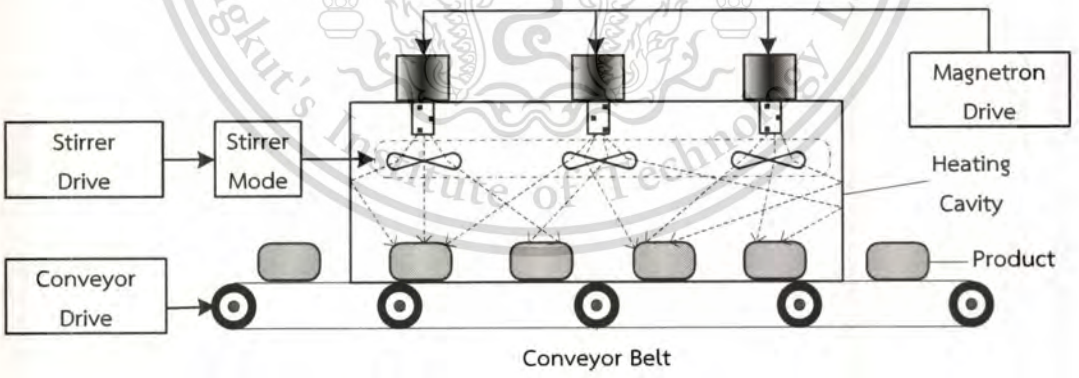


**Fig. 5.1** A conventional industrial microwave heating system with stirring mechanism

A typical microwave heating oven operates on the continuous wave mode with a magnetron tube as the source of radiation. The magnetron tube is an alternative heating source superior to the conventional heating method in which heat is transferred from outside to inside whereas the heat transfer principle is reversed in the microwave heating. Essentially, the magnetron tube converts an electric current

into electromagnetic radiation. A step-up transformer produces a high voltage to power the magnetron tube and rectifies a magnetron drive. The microwave energy from the magnetron tube is transferred through a waveguide section to the oven cavity, inside which stirrers and a conveyor belt create an even distribution of microwave radiation [23]. Figure 5.1 illustrates the conventional microwave heating system with stirring mechanism.

Microwave heating is a technique belonging to the family of electro-heat techniques, e.g. heat induction, radio frequency, direct resistance and infrared heating, which utilize the concept of electromagnetic waves. Many industries have adopted the microwave heating technique to replace the conventional heating method because the conventional heating system is bulky, difficult to operate and produces a non-uniform heat distribution [65, 66]. The major advantages of the microwave technology are rapid heat transfer, volumetric and selective heating, equipment compact size and ease of on-and-off switching. In the conventional microwave heating, the function of a stirrer in the cavity is either to evenly spread the microwave energy or to continually roll the materials over for even exposure to the microwave energy. The purpose of this dissertation is to develop a prototype of a non-stirring industrial microwave heating system.

The chaotic signals are the driving signal input of all magnetrons of the proposed system without a rotating mechanism inside the cavity. The advantages of chaotic signals are a wide frequency spectrum, fractal trajectories, and complex random.

## 5.2 The microwave carbonization

The microwave carbonization of biomass is a novel thermochemical technology in which microwave is used to irradiate the biomass. Compared to the conventional carbonization, the microwave carbonization offers more advantages, including ease of control, and lower consumption of time and energy. Thus, many industries have adopted and implemented the microwave carbonization [61]. However, one main issue with the microwave heating system is the non-uniform heat on biomass loads caused by the uneven electromagnetic distribution inside the

microwave cavity. The unevenness of electromagnetic distribution contributes to the hot spots, cold spots, thermal runaway panorama and low quality of product yields. This dissertation presents the design of a pilot-scale continuous biomass carbonization system using the multi-feed microwave heating. In addition, the chaotic pattern signals are utilized to regulate the radiation from each individual microwave source for a uniform heating distribution inside the carbonization reactor. The application of the chaotic pattern signals has found to improve the quality of the final products.

The typical carbonization temperature range for most biomass is 200-600 °C. In general, the design of a multi-feed microwave cavity must allow for the optimal control of the heating rate to improve heating uniformity [60-63]. Therefore, in this dissertation the multi-mode microwave radiation is adopted to heat the multi-feed microwave cavity, as illustrated in Figure. 5.2. The cavity is drilled to make two rows of five equally spaced rectangular openings each (i.e. a total of 10 openings). The openings are each fitted with a microwave source that contains a magnetron and a waveguide. In the center of the cavity is a vertical cement castable reactor, through which biomass to be reacted passes. The reactor is of cement so that the microwave radiation can penetrate.

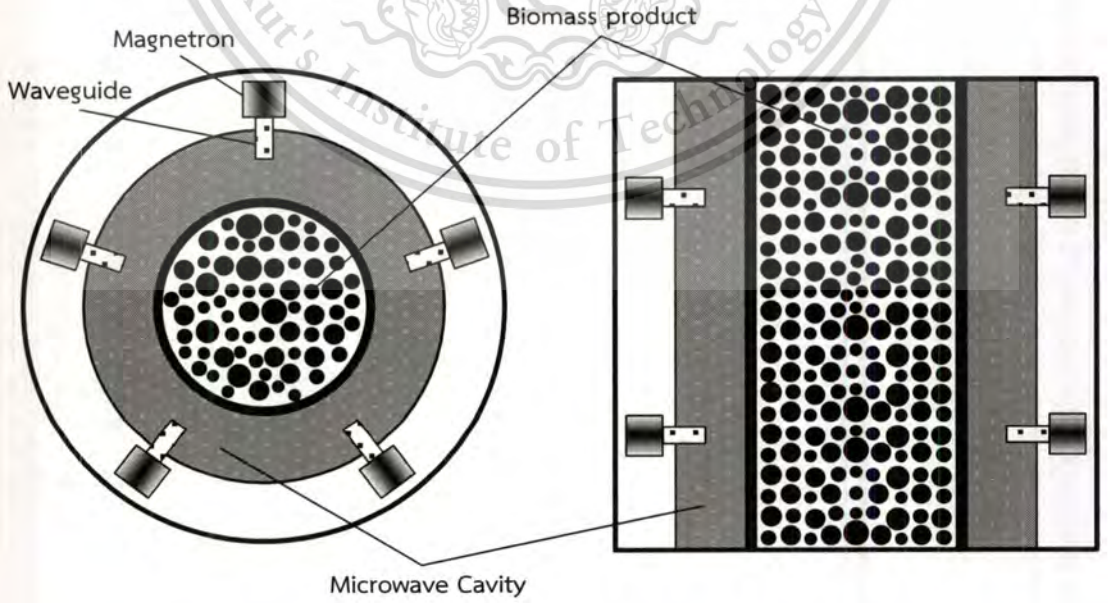


**Fig. 5.2** The multi-feed microwave cavity: Top view (left) and side view (right)

The proposed non-stirring microwave heating system enables an even distribution of heat throughout biomass. Since no stirrer is required, the design complexity and time required to construct the system are reduced. In fact, with the microwave reactor, a stirrer would bounce off the electromagnetic waves and thereby an uneven heat distribution inside the reactor. The waveguides in this dissertation are of the air-filled WR340 model with $a$ = 86 mm, $b$ = 43 mm and 211.5 mm in length, operating at 2.45 GHz with dominant TE10 mode.

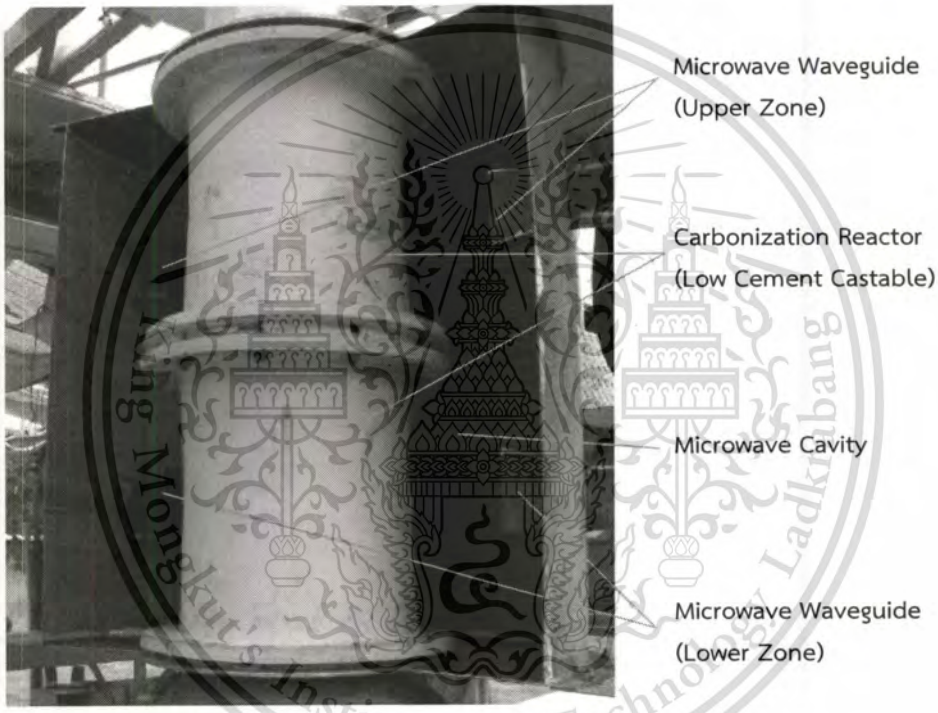


**Fig. 5.3** The carbonization reactor (upper and lower)

It is too complicated to determine the mode propagation inside the carbonization reactor based only on the waveguide properties due to varying dimensions and sizes of the materials passing through the reactor. Figure 5.4 shows photographs of the waveguide and components of the microwave heating system on the cavity exterior, while Figure 5.5 is the photo image of the microwave cooling units of the proposed microwave carbonization system.

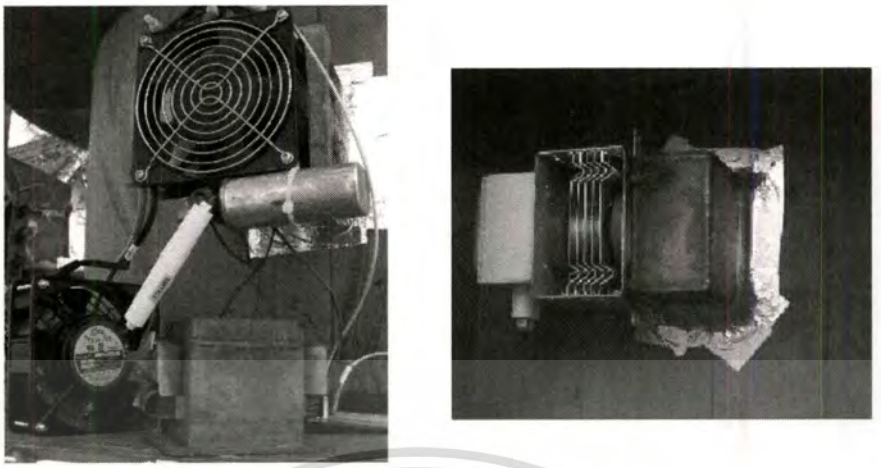

**Fig. 5.4** The waveguide and components of the microwave heating system

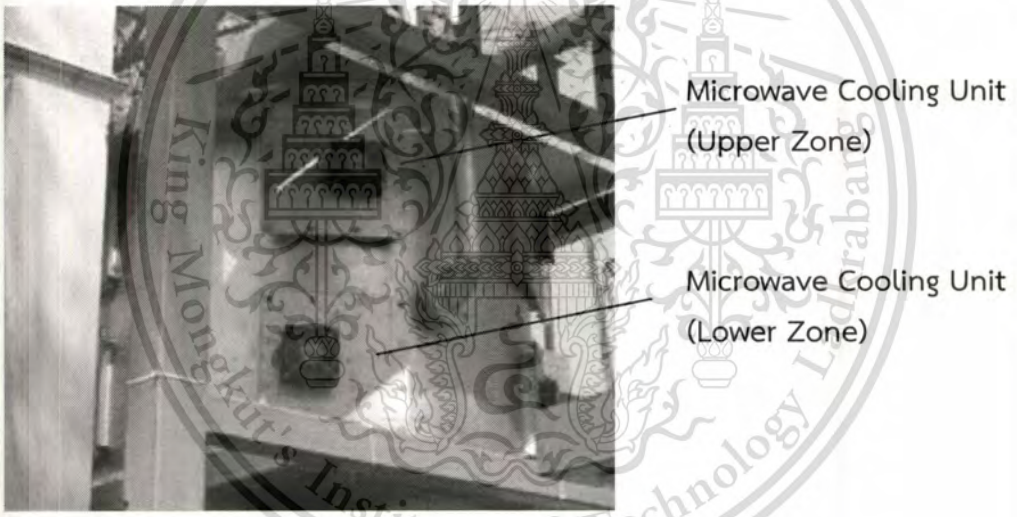


**Fig. 5.5** The microwave cooling units of the microwave carbonization system

## 5.3 Chaotic function

The chaotic signals are generated by an electronics circuit or by a computer simulation program. This section adopts the latter approach to simulate the chaotic signals based on the equations discussed in Chapter 3. The simulation chaotic signals are then used to determine the one-dimension-map, two-dimension-map and three-dimension-map Lyapunov exponents, as presented in Table 5.1. The positive Lyapunov exponents are selected to use in the experiments.

**Table 5.1** The Lyapunov exponents by chaotic equations

| Chaotic equations | Lyapunov exponent | | |
|---|---|---|---|
| | $\lambda_1$ | $\lambda_2$ | $\lambda_3$ |
| Logistic | **0.825** | - | - |
| Chua | 0.012 | 0.000 | -15.469 |
| Chen | **2.190** | 0.000 | -11.856 |
| Rossler | 0.072 | 0.000 | -5.572 |
| Sprott | 0.210 | 0.000 | -1.210 |
| Arnold | **1.570** | 0.000 | -11.856 |

## 5.4 Experiments

The proposed microwave carbonization system contains two rows of 5 magnetrons each, i.e. five for the upper row and another five for lower row, totaling ten magnetrons. The five magnetrons each in the upper and lower rows are termed M1, M3, M5, M7 and M9; and M2, M4, M6, M8, and M10, respectively. The experiments are carried out with dried coconut shells and consist of three stages:

First, four sequential radiating patterns (i.e. Patterns A, B, C and D) are selected to heat biomass load. In Pattern A, one magnetron (e.g. M1) is switched on for 5 minutes and turned off before another magnetron (M2) is ON for another 5 minutes and then OFF. The procedure continues until the last magnetron (M10) and at the end of 60 minutes, as shown in Figure 5.7. In Pattern B, two adjacent magnetrons (e.g. M1 & M2) are ON for 5 minutes and then OFF before the next pair (M3 & M4) is ON for another 5 minutes until the last pair (M9&M10) and the process restarts for a total length of time of 60 minutes (Figure 5.8). Pattern C is similar to Pattern B except that the pairs are not adjacent, e.g. M1&M6, M2&M7. The process repeats when the last pair M5&M10 is ON and continues for 60 minutes (Figure 5.9). In Pattern D, three magnetrons are ON at one time (e.g. M1, M4 & M7) for 5 minutes and then OFF before the another set of three magnetrons is switched ON and then OFF after 5 minutes. Once the last member of a set is M10 (e.g. M4, M7 & M10), the

process reverses until the last member is M1, the reversal occurs again. The process continues for a period of 60 minutes, as shown Figure 5.10. The temperatures inside the cavity achieved with four patterns of radiation are documented and compared.

Second, Pattern C is chosen due to high temperature generated although Pattern D generates the highest temperature as Pattern D requires highest power consumption. In addition, the temperatures of Patterns C and D are not significantly different. In the second stage, the length of time per radiation session is varied from 1/2, 1, 2, 3 to 5 minutes and the temperatures are taken. The total length of time remains unchanged at 60 minutes. The 2-minute radiation format is selected due to its highest resulting temperature.

Last, chaotic simulation patterns are applied to the 2-minute radiation session of Pattern C, resulting in the chaotic sequence of the ON magnetron pairs. The temperatures are taken continuously for 60 minutes.

### 5.4.1 Various patterns of microwave radiation

This research work experiments with four microwave radiation patterns (i.e. Patterns A, B, C and D) generated by the programmable logic control (PLC). Figure 5.6 shows the schematic of the microwave carbonization process of this research. In Pattern A, one magnetron (e.g. M1) is switched on for 5 minutes and turned off before another magnetron (M2) is ON for another 5 minutes and then OFF. The procedure continues until the last magnetron (M10) and at the end of 60 minutes, as shown in Figure 5.7. In Pattern B, two adjacent magnetrons (e.g. M1 & M2) are ON for 5 minutes and then OFF before the next pair (M3 & M4) is ON for another 5 minutes until the last pair (M9&M10) and the process restarts for a total length of time of 60 minutes (Figure 5.8). Pattern C is similar to Pattern B except that the pairs are not adjacent, e.g. M1&M6, M2&M7. The process repeats when the last pair M5&M10 is ON and continues for 60 minutes (Figure 5.9). In Pattern D, three magnetrons are ON at one time (e.g. M1, M4 & M7) for 5 minutes and then OFF before the another set of three magnetrons is switched ON and then OFF after 5 minutes. Once the last member of a set is M10 (e.g. M4, M7 & M10), the process reverses until the last

member is M1, the reversal occurs again. The process continues for a period of 60 minutes, as shown Figure 5.10. The temperatures inside the cavity achieved with four patterns of radiation are documented and compared.

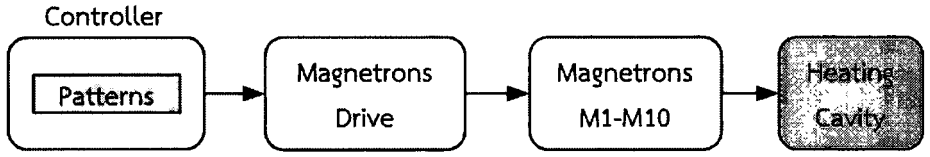


Fig. 5.6 The schematic of the microwave carbonization process

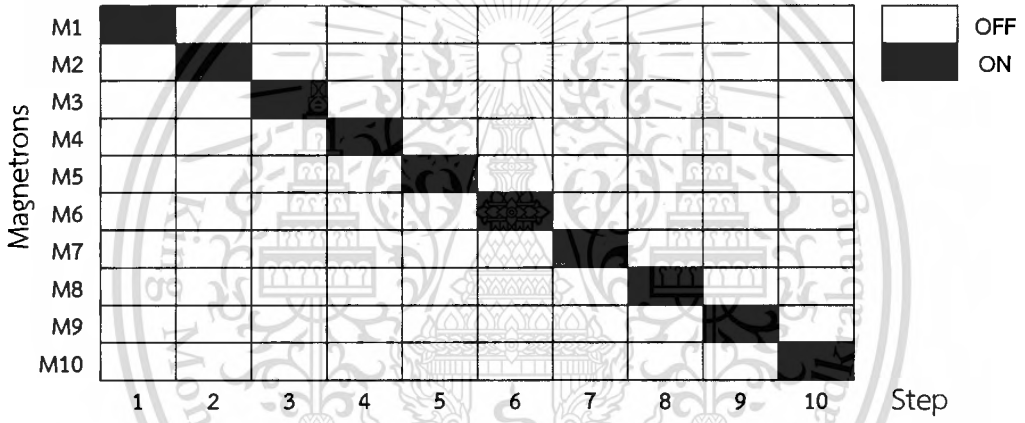


Fig. 5.7 The microwave radiation of Pattern A

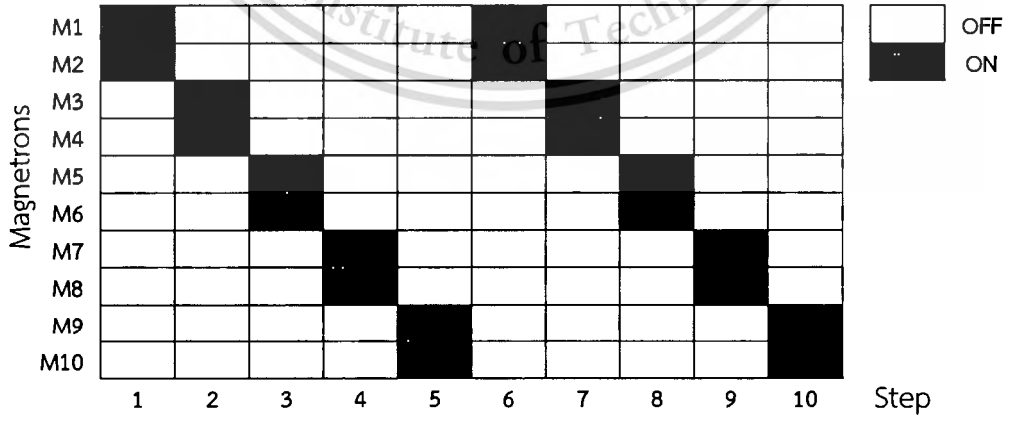


Fig. 5.8 The microwave radiation of Pattern B

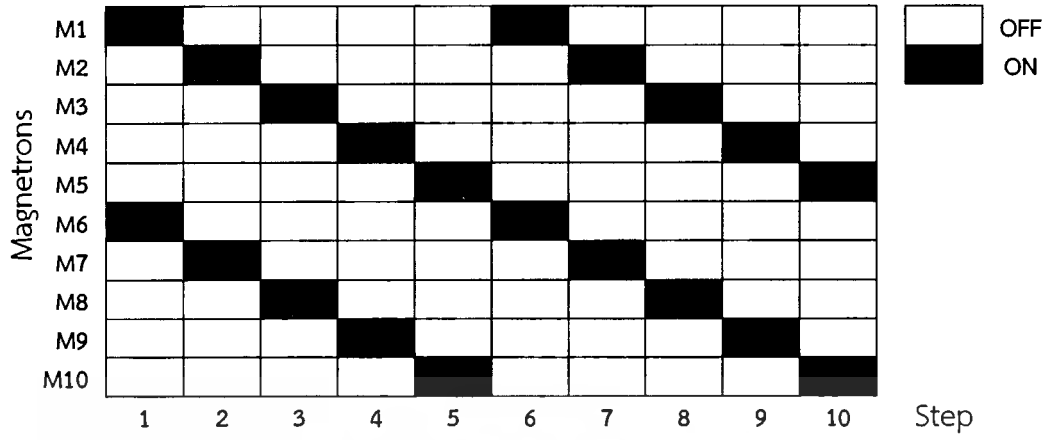


**Fig. 5.9** The microwave radiation of Pattern C

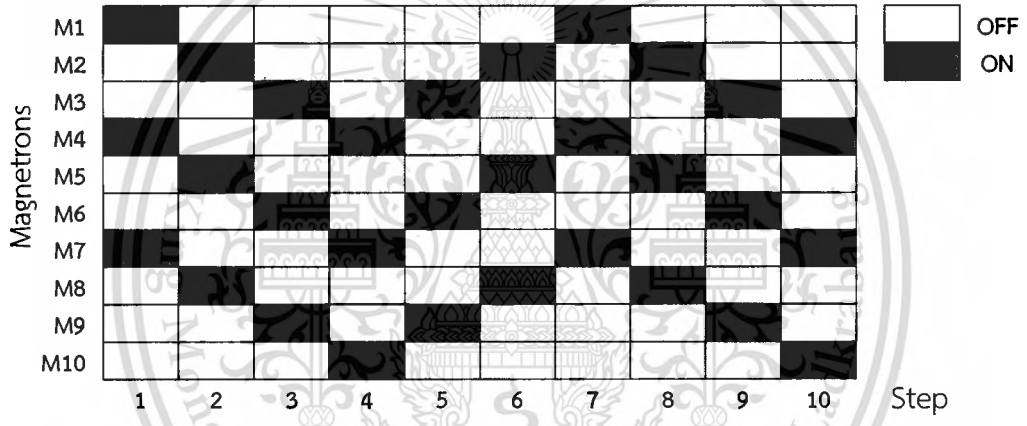


**Fig. 5.10** The microwave radiation of Pattern D

Figure 5.11 compares the resulting temperatures of four different microwave radiation patterns, i.e. Patterns A, B, C and D, for a period of 60 minutes. The temperatures of Patterns C and D are slightly different, but Pattern D consumes around 33% more power. Therefore, Pattern C is chosen for the experiment.

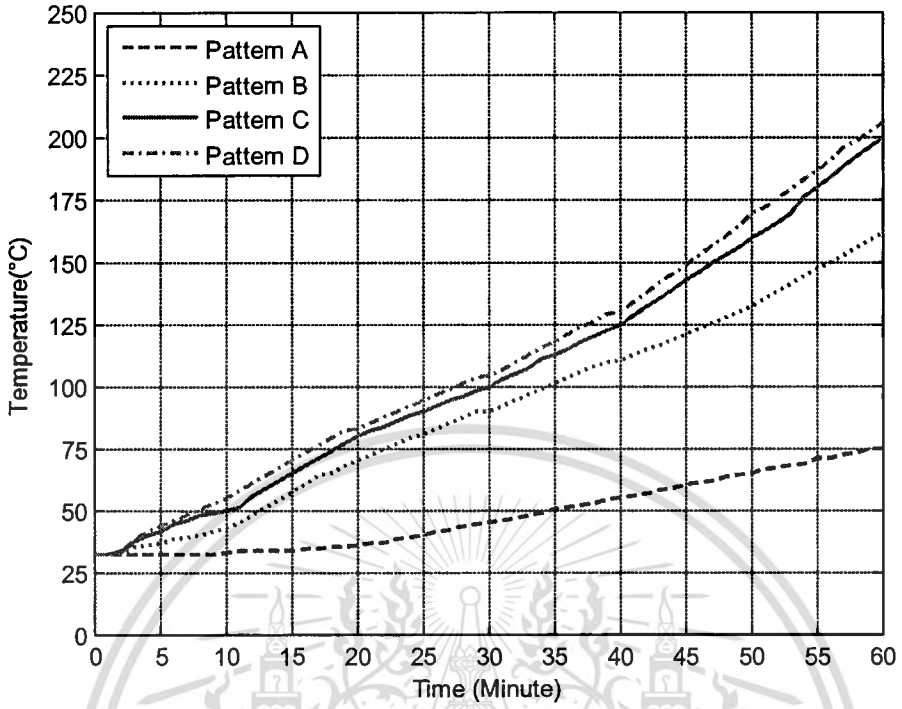


Fig. 5.11 The temperature comparison of four microwave radiation patterns

### 5.4.2 Various lengths of time of microwave radiation

The effects by varying time length per radiation session on temperature are investigated using the Pattern C radiation pattern due to the reason given above. The duration per radiation session is varied from 1/2, 1, 2, 3 to 5 minutes and the temperatures are taken. The total time duration remains unchanged at 60 minutes. Figure 5.12 illustrates the schematic of the microwave carbonization process with the time length per radiation session varied. Figure 5.13 compares the temperatures achieved with the varying radiation sessions of 1/2, 1, 2, 3 to 5 minutes for a total duration of 60 minutes. As seen in the figure, the 2-minute radiation session yields the highest temperature when used in conjunction with Pattern C. The 2-minute radiation session of Pattern C is chosen for experimenting with the chaotic patterns.

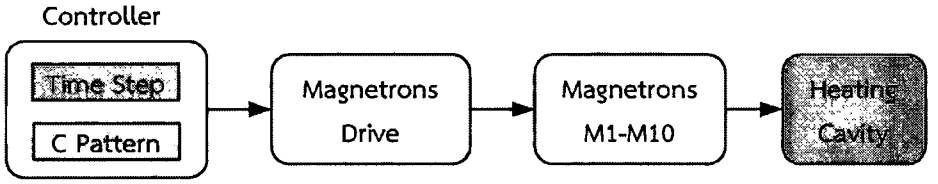


**Fig. 5.12** The schematic of microwave carbonization process with duration per session varied

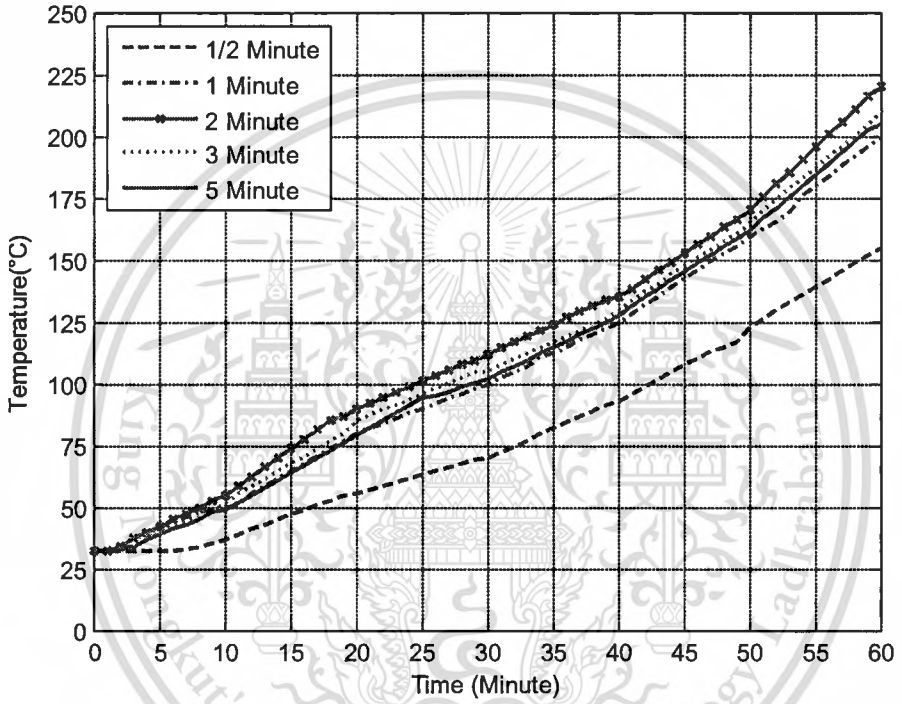


**Fig. 5.13** The comparison of temperatures achieved with varying radiation sessions

### 5.4.3 Chaotic mode of microwave radiation

Since it is difficult for microwave carbonization plants to implement the mechanical rotation or stirrer mode in the cavity, the chaotic behavior is applied to the microwave carbonization of the plants. Without the chaotic behavior, the biomass carbonization using Pattern C with 2-minute radiation session produces low quality charcoal products as a large volume of dried coconut shells are not carbonized. Nevertheless, the problem could be solved by introducing the chaotic behavior into the 2-minute radiation session of Pattern C. The chaotic equations

with large positive Lyapunov exponents (as presented Table 5.1) are chosen to generate chaotic behaviors. The chaotic equations chosen are the Logistic, Chen and Arnold chaotic functions.

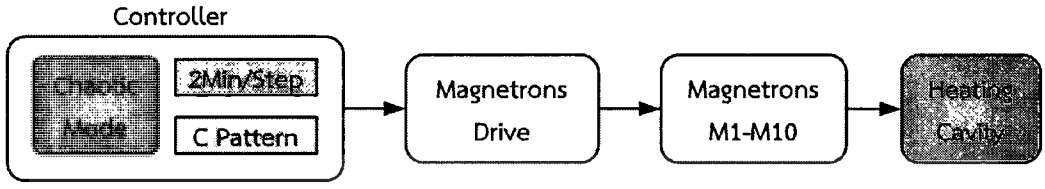


**Fig. 5.14** The schematic of microwave carbonization with addition of chaotic mode

Figure 5.14 shows the schematic of the microwave carbonization using the chaotic mode in conjunction with the 2-minute radiation session of Pattern C. The chaotic equations chosen to generate chaotic behaviors are the Logistic, Chen and Arnold chaotic functions. As seen in Figure 5.15, the Logistic chaotic function yields the highest temperature and thereby is selected as the chaotic function to generate the chaotic behaviors of the microwave radiation in the biomass carbonization.

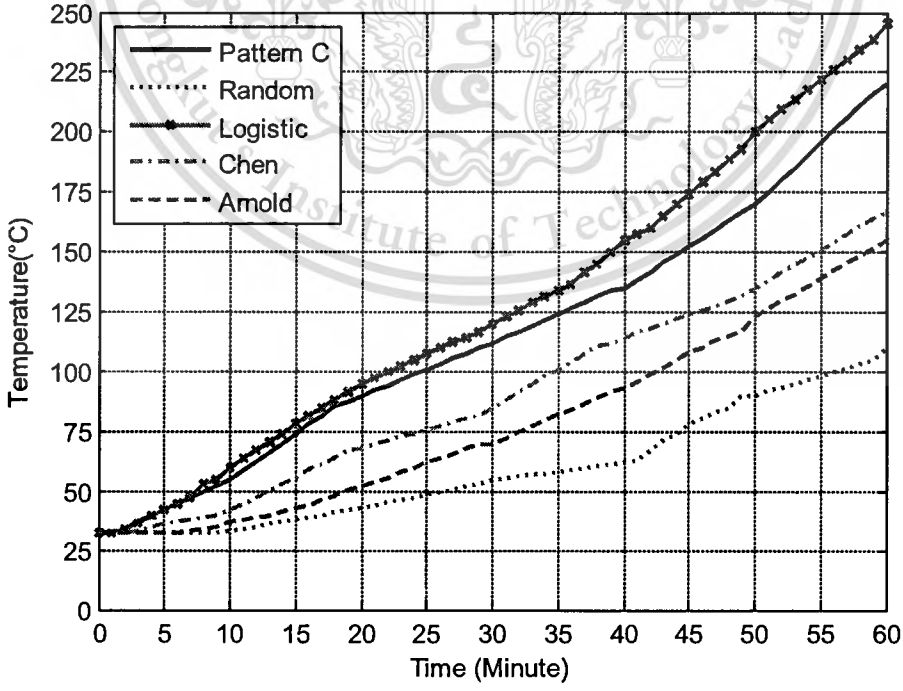


**Fig. 5.15** The comparison of temperatures achieved with various chaotic equations

## 5.5 The carbonization system using chaotic microwave radiation

Following the trial open-loop experiments of the carbonization system, the 2-minute radiation session of Pattern C using the Logistic function is selected and implemented in the carbonization plant under study. As previously reported, the Logistic chaotic function produces uniform microwave radiation. In general, the chaotic function is very sensitive to the initial condition parameter. To prove, the parameter $x_0$ of the Logistic function is altered by an increment of 0.00001 from 0.10000 until 0.10004. The temperatures and power consumption levels are taken.

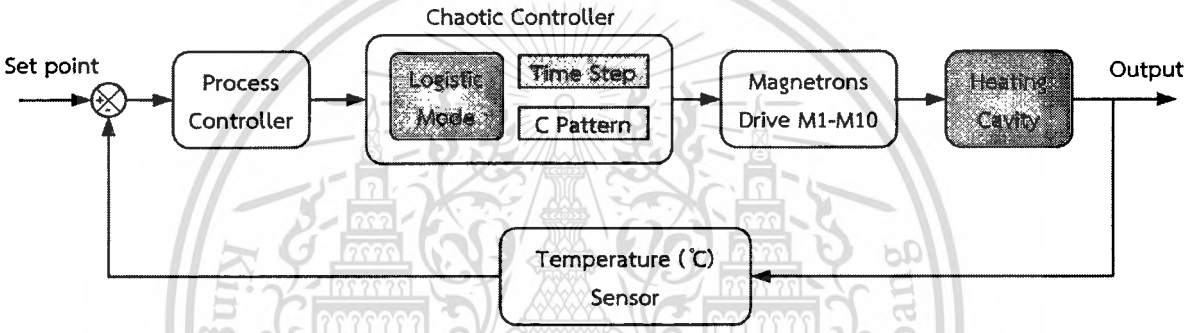


**Fig. 5.16** The schematic of the microwave carbonization process in a carbonization plant

Figure 5.16 shows a closed-loop microwave carbonization process by which the chaotic controller generates microwave and regulates the microwave radiation. The temperature of the cavity center is taken with a temperature sensor, which is compared against the set point temperature. If a temperature disparity exists, the process controller sends a command to the chaotic controller to switch it on or off. Generally, at the startup all magnetrons are switched on until the set point temperature is reached prior to the activation of the chaotic controller. In Figure 5.17 shows a normalized $f(x)$ of parameter $x_0$ of the Logistic function $f(x) = ax(1-x)$ at $a$ = 3.8. The $x_0$ parameter of the Logistic function is altered by an increment of 0.0001, starting from 0.10000 to 0.10004. The temperatures and power consumption levels are measured for the $x_0$ values.

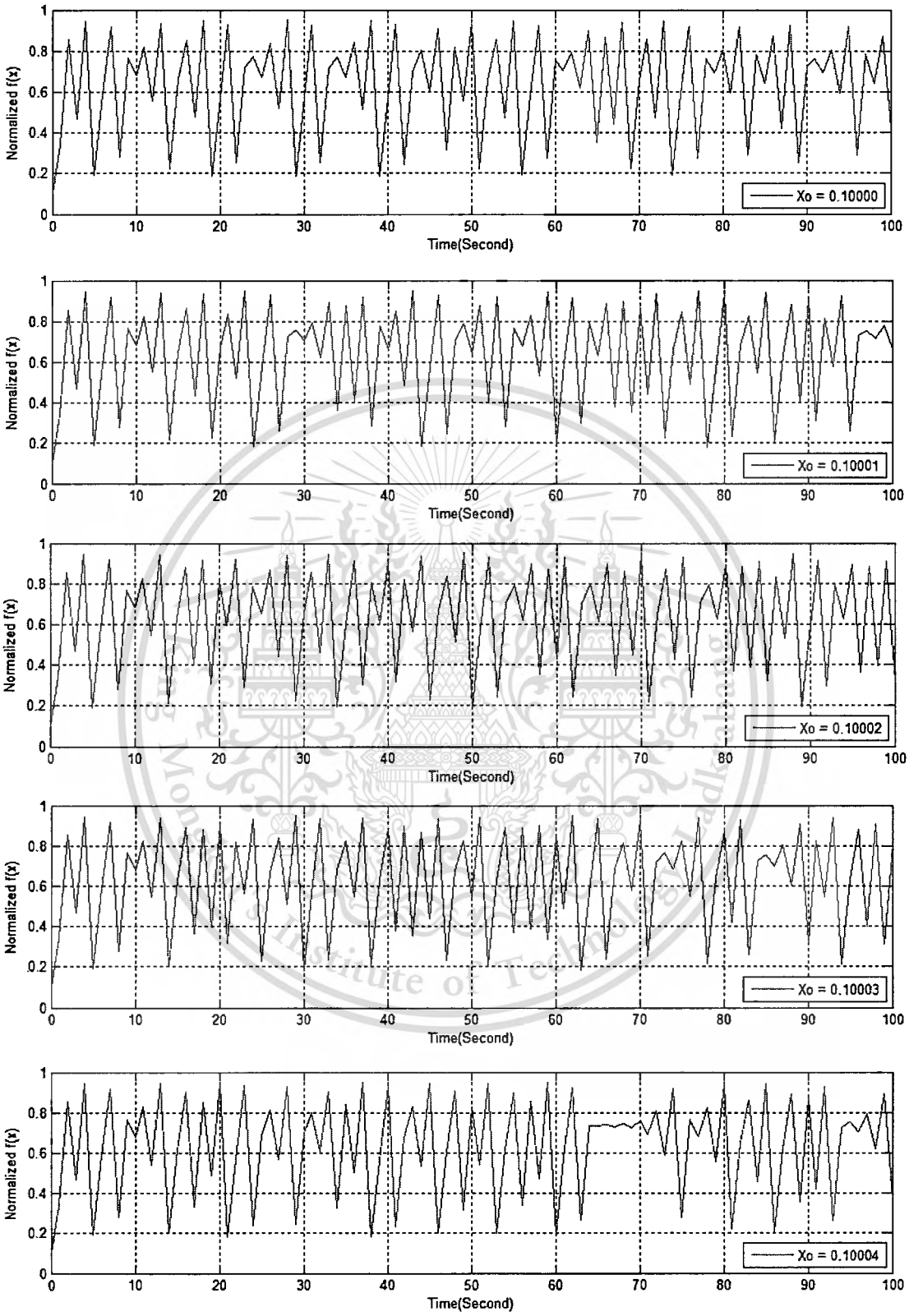


**Fig 5.17** The normalized $f(x)$ of parameter $x_0$ of the Logistic function

**Table 5.2** The activated magnetrons by ranges of Logistic function values

| $f(x)$ | ≤ 0.2 | 0.2>,≤ 0.4 | 0.4>,≤ 0.6 | 0.6>,≤ 0.8 | 0.8>,≤1.0 |
|---|---|---|---|---|---|
| ON magnetrons | M1 , M6 | M2 , M7 | M3 , M8 | M4 , M9 | M5 , M10 |

The set-point temperature of the carbonization system is 450°C for a total period of 180 minutes. As shown in Table 5.2, the sequence of activated magnetrons is regulated by the normalized $f(x)$ of $x_0$ of the Logistic function. Figure 5.18 depicts the comparison results of different $x_0$ of the Logistic function in terms of temperature and time. As shown in Figure 5.18, the different values of $x_0$, which are generated by the Logistic chaotic equation, have similar heating temperature characteristics but different power consumption levels. The least power consumption was identified at $x_0$ = 0.10003.

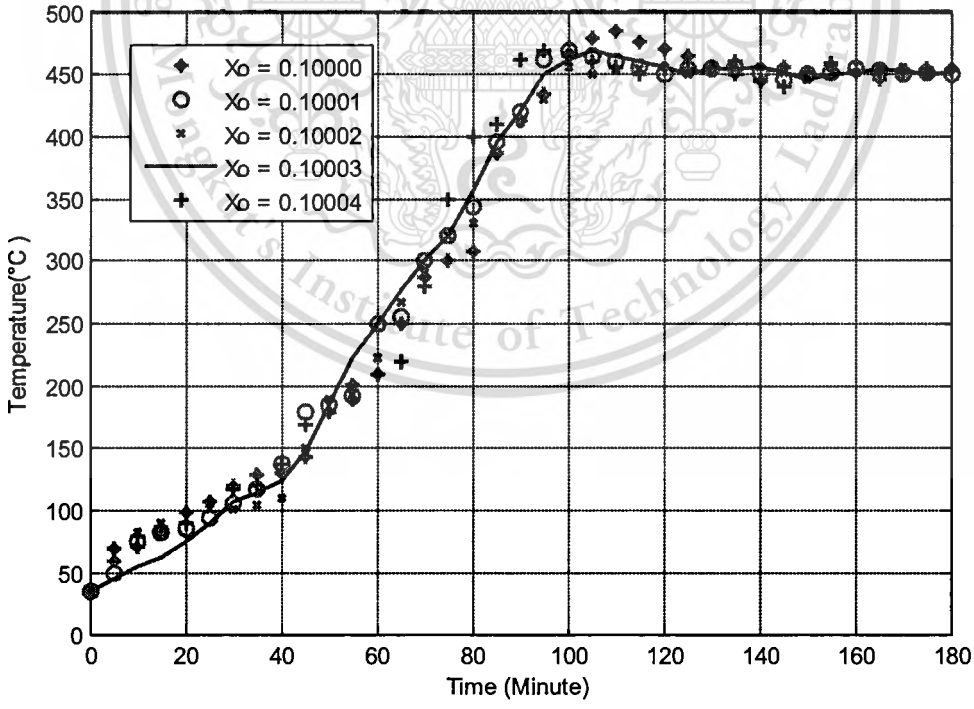


**Fig. 5.18** The comparison of different $x_0$ of the Logistic function in terms of temperature and time

The comparison of the electric power consumption levels from the startup period through the entire operating period of 180 minutes of five different values of $x_0$ is presented in Figure 5.19. It is found that $x_0$ = 0.10003 consumes the least power while generating the heating temperature similar to the temperatures generated by the other $x_0$ values.

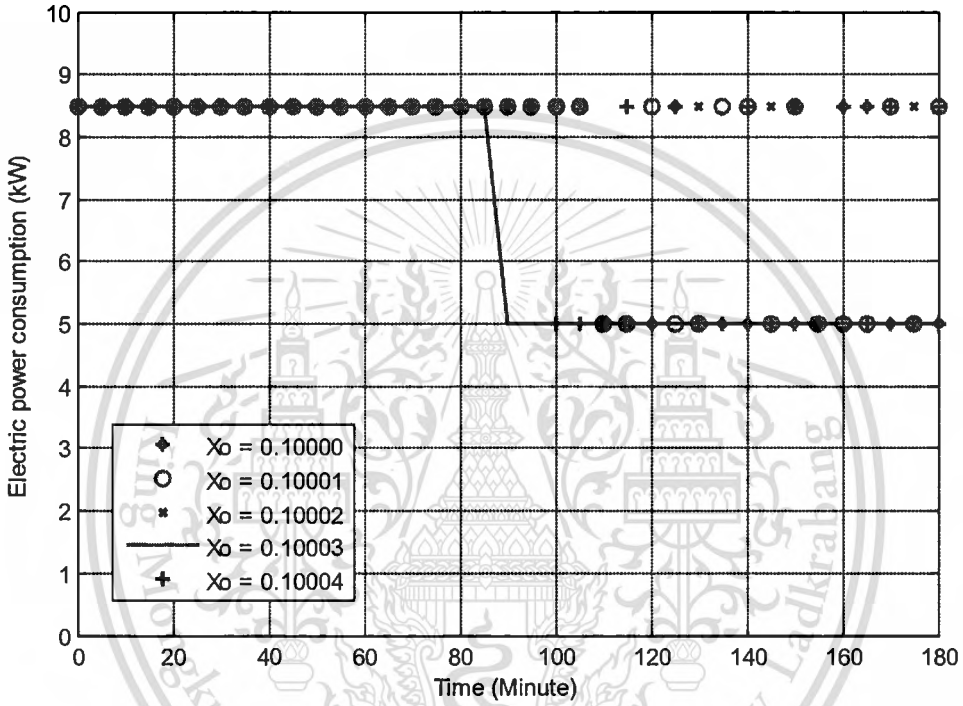


**Fig. 5.19** The electric power consumption of different $x_0$ from the startup through the entire operating period

Table 5.3 presents the power consumption levels of the five $x_0$ values. The table shows the average electric power consumption by varying the $x_0$ parameter. The power consumption is smallest (5.94 kW/h) when $x_0$ = 0.10003.

**Table 5.3** The average electric power consumption from the startup through the end period of 180 minutes of different $x_0$

| Logistic parameter ($x_0$) | 0.10000 | 0.10001 | 0.10002 | 0.10003 | 0.10004 |
|---|---|---|---|---|---|
| Average power (kW/h) | 6.39 | 6.93 | 6.57 | 5.94 | 6.84 |

## 5.6 Summary

This chapter presents the chaotic application for industrial microwave heating in the carbonization system without stirring mechanism. The Logistic function at $a$ = 3.8 and $x_0$ = 0.10003 are selected to generate the chaotic sequence for microwave radiation. The implemented microwave radiation is of Pattern C in which a pre-determined pair of magnetrons (i.e. 2 magnetrons) after one another is activated for 2 minutes per session. The adoption of the pattern helps minimize the quantity of non-uniform charcoal outputs and lowers the electric power consumption. The following chapter touches on the conclusions, discussions and future work relating to the oscillation and chaotic application on a much larger industrial scale.

# Chapter 6
# Conclusions

## 6.1 Conclusions

This dissertation presents the novel oscillation applications on an industrial scale: the periodic oscillation and chaotic oscillation applications.

### 6.1.1 Periodic oscillation application

The periodic oscillation application was discussed in Chapter 4 and demonstrated with the basic mechanical oscillator, which is the tuning fork with piezoelectric resonator (TFP) at a 3 kHz resonance frequency. A needle was mounted onto the TFP. An increase of mass with the needle mounting induces errors that can be rectified by an addition of electronic components and a software program to improve the $Q$ factor. The modified TFP is well applicable to classification of elastic nano-scale materials by comparing the phase difference between input and output signals. In the experiments, the depths of contact point between the surface of elastic materials and the probe tip were increased from micrometer-scale to nanometer-scale increments. The method is capable of producing precise and reliable measurements for classification of nano-scale materials and is also repeatable.

### 6.1.2 Chaotic oscillation application

The chaotic oscillation application was detailed in Chapter 5. The chaotic patterns are generated by a simulation program and chaos behaviors are confirmed by the positive Lyapunov exponents and bifurcation diagrams. The chaotic equations to generate the chaotic patterns are simple and require no fabrication of hardware. The most suitable chaotic pattern for uniform microwave heating inside the reactor is the Logistic map of $a$ = 3.8 and $x_0$ = 0.10003 as an initial parameter. This chaotic pattern can be adopted to improve the process temperature characteristic, process power consumption and carbonization charcoal yield. In addition, the chaotic patterns could be a good alternative to the conventional industrial heating method. Appendix A and B presents photographs of a real microwave heating carbonization plant.

## 6.2 Discussions

The modified TFP with periodic oscillation is able to classify the elastic nano-scale materials and to sensing mechanical nano-scale vibrations. This method operates on the phase difference principle [18-20] with an addition of the $Q$ factor and phase control.

The chaotic oscillation can be applied to a carbonization process with multi-feed microwave heating without stirring mechanism. The output yields of the conventional carbonization process are of low quality as the temperature inside the rector is non-uniform [21-23]. The chaotic microwave heating can tackle this problem of low quality product yields.

## 6.3 Future work

A tuning fork with piezoelectric of precise sensing capability can be fabricated with little investment. The fabricated tuning fork can be applied to measurement of micro-scale vibrations and micro-scale fluid rates. In addition, it can be used in the nano-scale measurement of an industrial scale without the need for complex devices.

The industrial application of chaotic behavior is not limited only to microwave eating but the chaotic behavior can be applied to various tasks, such as in the chemical mixing systems, in data encryption for high level security.

# References


[1] J. Gleick, "Chaos: Making a new science," Viking Penguin, New York, 1987.

[2] H. Nagashima and Y. Baba, "Introduction to chaos physics and physics and mathematics of chaotic phenomena," Institute of physics publishing, 1999.

[3] S.H. Strogatz, "Nonlinear dynamics and chaos with applications to physics, biology, chemistry and engineering," Addison-Wesley publishing, 1996.

[4] A. Jansri, K. Klomkarn and P. Sooraksa, "Further investigation on trajectory of chaotic guiding signals for robotic systems," *IEEE International Symposium on Communications and Information Technology*, Vol.2, October 2004, pp.1166–1170.

[5] Z. Zhang, and G. Chen, "Chaotic motion generation with applications to liquid mixing," *Proceedings European Conference on Circuit Theory and Design*, Vol.1, 2005, pp. 225 – 228.

[6] Z. Zhang, and G. Chen, "Liquid mixing enhancement by chaotic perturbations in stirred tanks," *Chaos Solution & Fractals*, Vol.36, 2008, pp. 144-149.

[7] S. Ye, and K.T. Chau, "Chaoization of DC Motors for Industrial Mixing," *IEEE Transactions on Industrial Electronics,* Vol.54, 2007, pp. 2024-2032.

[8] S. Ye and K.T. Chau, "Destabilization control of a chaotic motor for industrial mixers," *Industry Applications Conference,* Vol.3, 2005, pp.1724–1730.

[9] M.Gaczynska and P.A. Osmulski, "AFM of biological complexes: What can we learn?," *Current Opinion in Colloid & Interface Science*, Vol. 13, No 5, 2008, pp. 351–367.

[10] C.S. Lin, C.Y. Wu, H.C. Hsu, K.M.C. Li, and L. Lin "Rapid bio-test strips reader with image processing technology," *International Journal for Light and Electron Optics*, 2004, pp. 363-369.

[11] A. Benoit, A. Caplier, B. Durette, J. Herault "Using Human Visual System modeling for bio-inspired low level image processing," *Computer Vision and Image Understanding*, July 2010, pp. 758-773.

[12] A. Beghdadi, M.C. Larabi, A. Bouzerdoum, K.M. Iftekharuddin "A survey of perceptual image processing methods," *Signal Processing: Image Communication*, September 2013, pp. 811-831.

[13] R. Blaauwgeers, M. Blazkova, M. Clovecko, V.B. Eltsov, R.D. Graaf, J. Hosio, M. Krusius, D. Schmoranzer, W. Schoepe, L. Skrbek, P. Skyba, R.E. Solntsev, and D.E. Zmeev, "Quartz Tuning Fork: Thermometer, Pressure and Viscometer for Helium Liquids," *Journal of Low Temperature Physics*, 2007, pp. 537-562.

[14] S. Dutta, S.K. Pal, S. Mukhopadhyay, R. Sen "Application of digital image processing in tool condition monitoring," *CIRP Journal of Manufacturing Science and Technology*, Vol 6, 2013, pp. 212-232.

[15] H. Lee, D. Lee, K.B. Kim, Y. Seo, H. Kim, and H. Lee "Real-time atomic force microscopy in lubrication condition," *Ultramicroscopy*, Vol. 110, June 2010, pp. 826-830.

[16] H. Melikyan, T. Sargsyan, A. Babajanyan, S. Kim, J. Kim, K. Lee, and B. Friedman, "Hard disk magnetic domain nano-spatial resolution imaging by using a near-field scanning microwave microscope with an AFM probe tip," *Journal of Magnetism and Magnetic Materials*, Vol. 321, No. 16, August 2009, pp. 2483–2487.

[17] D. Lee, H. Lee, N.S. Lee, K.B. Kim and Y. Seo, "High-speed atomic force microscopy with phase-detection," *Current Applied Physics*, Vol.12, No.3, May 2012, pp. 989–994.

[18] L. Gonzalez, J. Otero, G. Cabezas and M. Puig-Vidal, "Electronic driver with amplitude and quality factor control to adjust the response of quartz tuning fork sensors in atomic force microscopy applications," *Sensors and Actuators A: Physical*, Vol. 184, Sep 2012, pp. 112–118.

[19] D. Bayat, T. Akiyama, N. F. de Rooij and U. Staufer, "Dynamics Behavior of the Tuning Fork AFM Probe," *Micro Electronic Engineering*, Vol. 85, 2008, pp. 1018-1021.

[20] M. Hofer, S. Adamsmaier, T. S. Van Zanten, L. A. Chtcheglova, C. Manzo, M. Duman, B. Mayer, A. Ebner, M. Moertelmaier, G. Kada, M. F. Garcia-Parajo, P. Hinterdorfer and F. Kienberger, "Molecular Recognition Imaging using Tuning Fork-Based Transverse Dynamic Force Microscopy," *Ultramicroscopy*, Vol. 110, 2010, pp. 605-611.

[21] P. Payakkawan, "Continuous Biomass Carbonization System using Chaotic Microwave Heating," Ph.D Dissertation, King Mongkut's Institute of Technology Ladkrabang, 2013.

[22] T. V. C. T. Chan and H. C. Reader,"Understanding Microwave Heating Cavities," Artech House Publishers, 2000.

[23] M. Gupta, E. Wong, and W. Leong, "Microwaves and Metals," John Wiley & Sons, 2010.

[24] K. Aihara and R. Katayama, "Chaos engineering in Japan," *Communication ACM*, Vol. 38, No. 11, 1995, pp. 103–107.

[25] T. Miyano, S. Kimoto, H. Shibuta, K. Nakashima, Y. Ikenaga, and K. Aihara, "Time series analysis and prediction on complex dynamical behavior observed in a blast furnace," *Physica D: Nonlinear Phenomena*, Vol. 135, January 2000, pp. 305-330.

[26] K. Aihara and R. Katayama, "A special issue on chaos engineering," *Journal of Intelligent Fuzzy System*, Vol. 5, No. 1, 1997, pp. 1–2.

[27] E. Saatdjian, A.J.S. Rodrigo, and J.P.B. Mota, "A study of mixing by chaotic advection in two three-dimensional open flows," *Chemical Engineering Science*, Vol. 81, October 2012, pp. 179-190.

[28] N. Gui, J. Fan, and K. Cen, "A macroscopic and microscopic study of particle mixing in a rotating tumbler," *Chemical Engineering Science*, Vol.65, May 2010, pp. 3034-3041.

[29] Z. Wang and K.T. Chau, "Design, Analysis, and Experimentation of Chaotic Permanent Magnet DC Motor Drives for Electric Compaction," *IEEE Transactions on Circuits and Systems*, Vol.56, 2009, pp.245-249.

[30] S.H. Strogatz, "Sync:The Emerging Science of Spontaneous Order," Penguin UK, 2003, pp 106-109.

[31] F.S. Crawford, "Waves Berkeley Physics Course," Vol. 3, McGraw-Hill, New York, 1968.

[32] A. Hirose, and K.E. Lonngren, "Introduction to Wave Phenomena," John Wiley & Sons, New York, 1985.

[33] H.J. Pain, "The Physics of Vibrations and Waves," John Wiley & Sons, Chichester UK, 1999.

[34] W. Scott, "Vibrations of Cantilever Beams: Deflection, Frequency, and Research Uses," University of Nebraska–Lincoln, 1999.

[35] S.M. Han, H. Benaroya, and T. Wei, "Dynamics of transversely vibrating beams using four engineering theories," *Journal of Sound and Vibration*, Vol.225, 1999, pp. 935-988.

[36] J.M. Friedt and E. Carry, "Introduction to the quartz tuning fork," *American Journal of Physics*, Vol. 75, No. 5, May 2007, pp. 415-422.

[37] K. Hirose, Y. Irie, S. Hirata and H. Aoyama, "Micro Gap Measurement by Vibration Mode for Needle-type dispenser," *Proceeding of the 2011 IEEE International Conference on Mechatronics and Automation*, Beijing, China August 2011, pp. 555-560.

[38] H. Hida, M. Shikida, K. Fukuzawa, S. Murakami, Ke. Sato, K. Asaumi, Y. Iriye, and K. Sato, "Fabrication of a quartz tuning-fork probe with a sharp tip for AFM systems," *Sensors and Actuators A: Physical*, Vol. 148, November 2008, pp. 311-318.

[39] R .Nishi, I. Houda, T. Aramata, Y. Sugawara, and S. Morita, "Phase change detection of attractive force gradient by using a quartz resonator in noncontact atomic force microscopy," *Applied Surface Science*, Vol. 157, April 2000, pp. 332-336.

[40] M. Barbic, L. Eliason, and J. Ranshaw, "Femto-Newton force sensitivity quartz tuning fork sensor," *Sensors and Actuators A: Physical*, Vol.136, May 2007, pp. 564-566.

[41] T.D Rossing, D.A. Russell, and D.E. Brown, "On the acoustics of tuning forks," *American Association of Physics Teachers,* Vol.60, July 1972, pp. 620-626.

[42] C.Y.J. Wang, and G.C. Tsai, "A Study of Small Sized Quartz Tuning Fork Using Finite Element Analysis," *Workshop on Future Frequency Control Devices*, December 2008, pp. 1-5.

[43] D. B. Nowak, "The Design of a Novel Tip Enhanced Near-field Scanning Probe Microscope for Ultra-High Resolution Optical Imaging," Ph.D Dissertation, Portland State University, 2010.

[44] "Piezoelectric Quartz Tuning Forks for Scanning Probe Microscopy," *Nanonis GmbH*, Switzerland, 2005.

[45] P. Glendinning, "Stability, Instability and Chaos," Cambridge University Press, 1994.

[46] K.T. Alligood, T.D. Sauer, and J.A. Yorke, "Chaos and introduction to dynamical systems," Springer-Verlag, New York, 1997.

[47] G.L. Baker, and J.P. Gollub, "Chaotic dynamics on introduction," Cambridge University Press, 1990.

[48] R.C. Hilborn, "Chaos and nonlinear dynamics," Oxford University Press, 2000.

[49] A.b. Cambel, "Applied chaos theory a paradigm for complexity," Academic press, 1993.

[50] K.T. Chau and Z. Wang, "Chaos in electronic drive systems analysis, control and application," John Wiley & Sons, 2011.

[51] N.V. Kuznetsov and G.A. Leonov, "On stability by the first approximation for discrete systems," *International Conference on Physics and Control*, 2005, pp. 596–599.

[52] J.C. Sprott, "Chaos and Time-Series Analysis," Oxford University Press, 2003.

[53] R.M May, "Simple mathematical models with very complicated dynamics." *Nature,* Vol. 261, June 1976, pp. 459-467.

[54] K. Briggs, "A Precise Calculation of the Feigenbaum Constants," *Mathematics of Computation, American Mathematical Society*, Vol.57, No.195, July 1991, pp. 435–439.

[55] F.C. Moon, "Chaotic and fractal dynamics : an introduction for applied scientists and engineers," John Wiley, New York, 1992.

[56] C. Mira, "Chaotic Dynamics in Two-Dimensional Noninvertible Maps," World Scientific Series on Nonlinear Science Series A, Vol. 20, 1996.

[57] H.G. Schuster, "Deterministic Chaos: An Introduction," John Wiley & Sons, 1995.

[58] J. Pritchard, "The chaos cookbook : a practical programming guide," Oxford : Butterworth Heinemann, 1996.

[59] M. Cencini, F. Cecconi, and A. Vulpiani, "Chaos: From Simple Models to Complex Systems," World Scientific, 2010.

[60] A. Oloyede and P. Groombridge, "The influence of microwave heating on the mechanical properties of wood," *Journal of Materials Processing Technology*, Vol.100, 2000, pp 67-73.

[61] T.J. Appleton, R.I. Colder, S.W. Kingman, I.S. Lowndes, and A.G. Read, "Microwave technology for energy-efficient processing of waste," *Applied Energy*, Vol. 81, 2005, pp. 85-113.

[62] M.P. Forrer, "A flexure-mode quartz for an electronic wrist-watch,"*23rd Annual Symposium on Frequency Control*, 1969, pp. 157-162.

[63] H. Li, C. Du, and Y. Wang, "Opimal Reset Control for A Dual-Stage Actuator System in HDDs," *IEEE Transactions on Mechatronics*, Vol. 16, No. 3, June 2011, pp. 480-488.

[64] C.K. Pang, F.L. Lewis, S.S. Ge, G. Guo, B.M. Chen and T.H. Lee, "Sigular Perturbation Control for Vibration Rejection in HDDs Using the PZT Active Suspension as Fast Subsystem Observer," *IEEE Transactions on Industry Electronics*, Vol. 54, No. 3, June 2007, pp. 1375-1386.

[65] M. Mehdizadeh, "Microwave/RF Applicators and Probes for Material Heating, Sensing, and Plasma Generation," A Design Guide, Elsevier, 2010.

[66] A. Balestrino, F. Bassini, and P. Pelacchi, "On the control of a pyrolysis process," *International conference on clean electrical power,* 2007, pp 409-414.

# Appendix A

The pilot-scale microwave carbonization system

# Appendix A

The pilot-scale microwave carbonization system using multi-feed microwave heating without stirring mechanism.

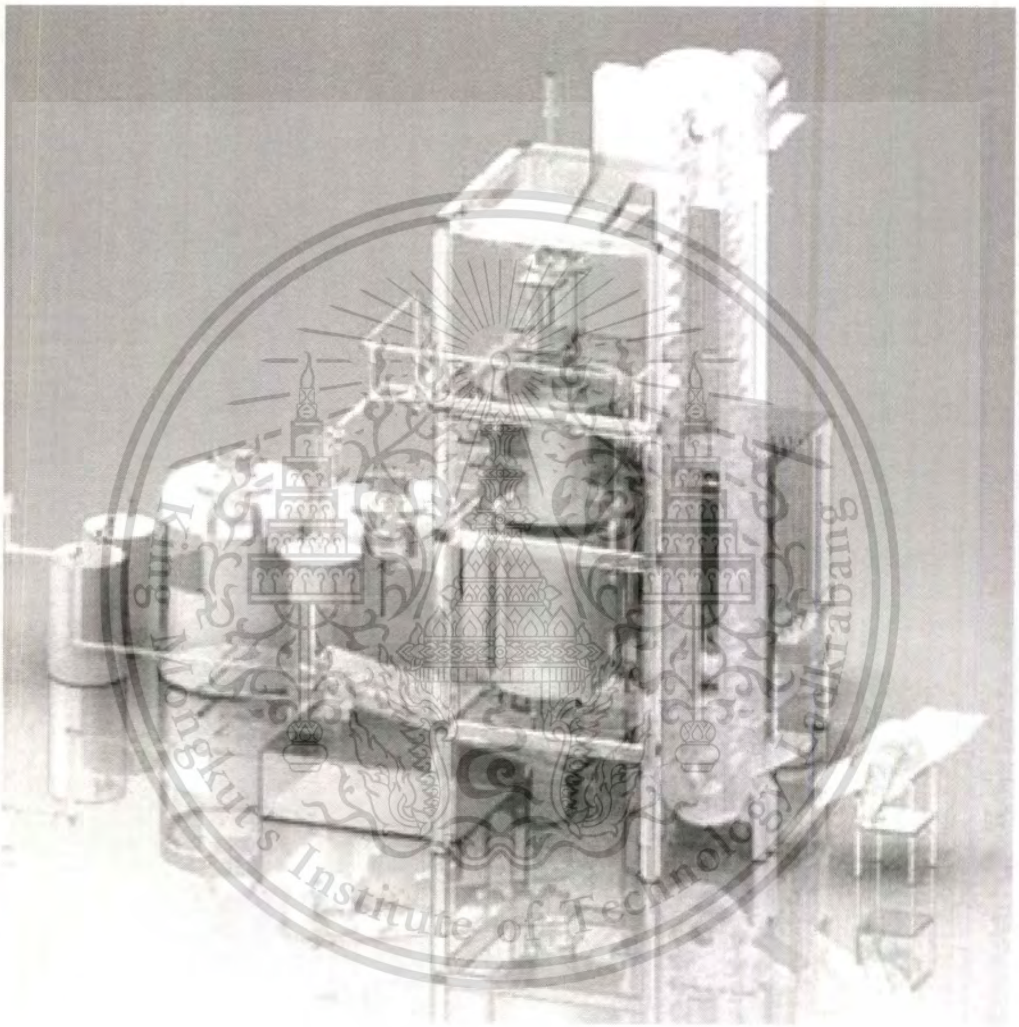

**Fig. a.1** The 3D design of the microwave carbonization system

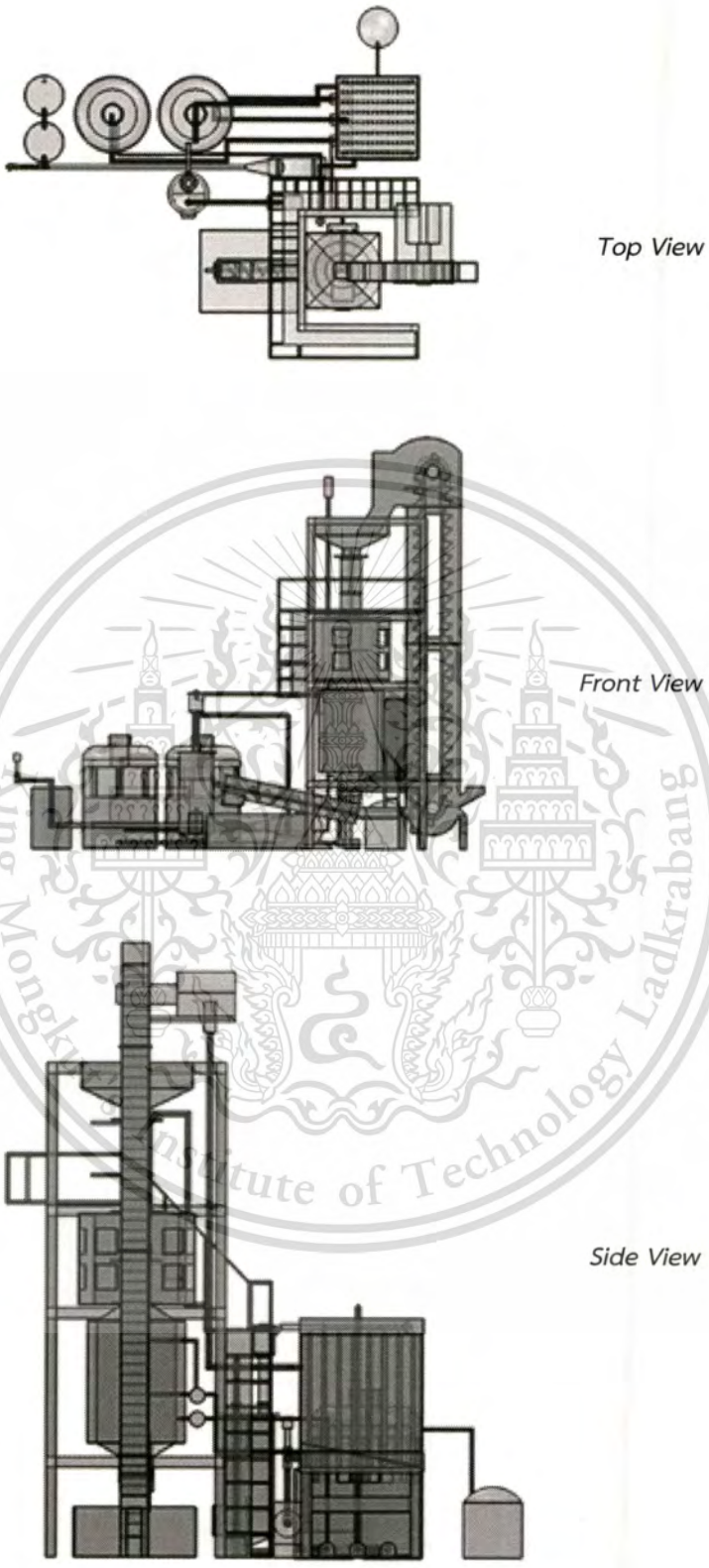


**Fig. a.2** The top, front and side views of the microwave carbonization system

# Appendix B

The microwave carbonization plant

# Appendix B

The essential parts and components of the pilot-scale microwave carbonization system using multi-feed microwave heating without stirring mechanism.

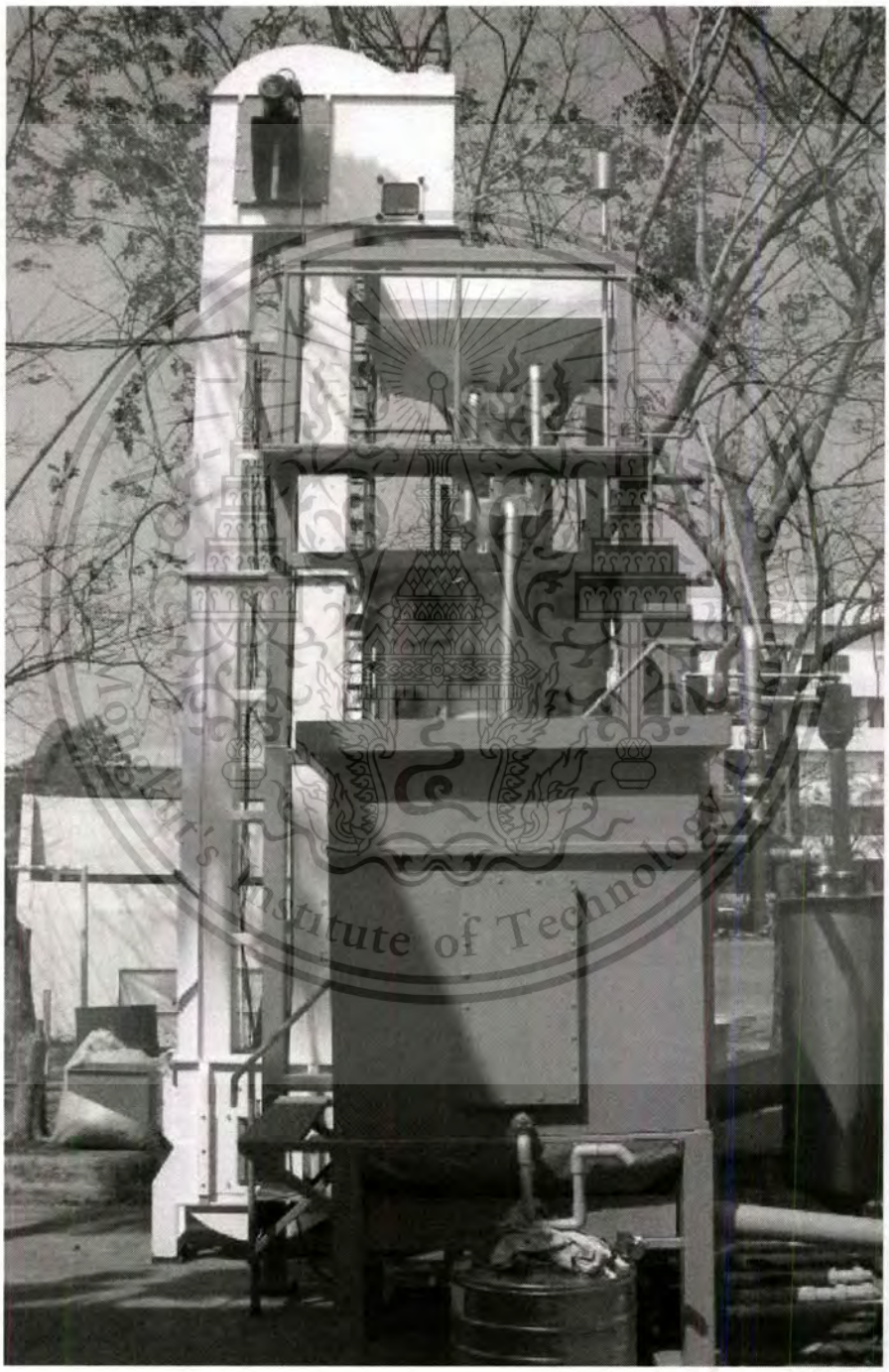

**Fig. b.1** The microwave carbonization plant (1)

**Fig. b.2** The microwave carbonization plant (2)

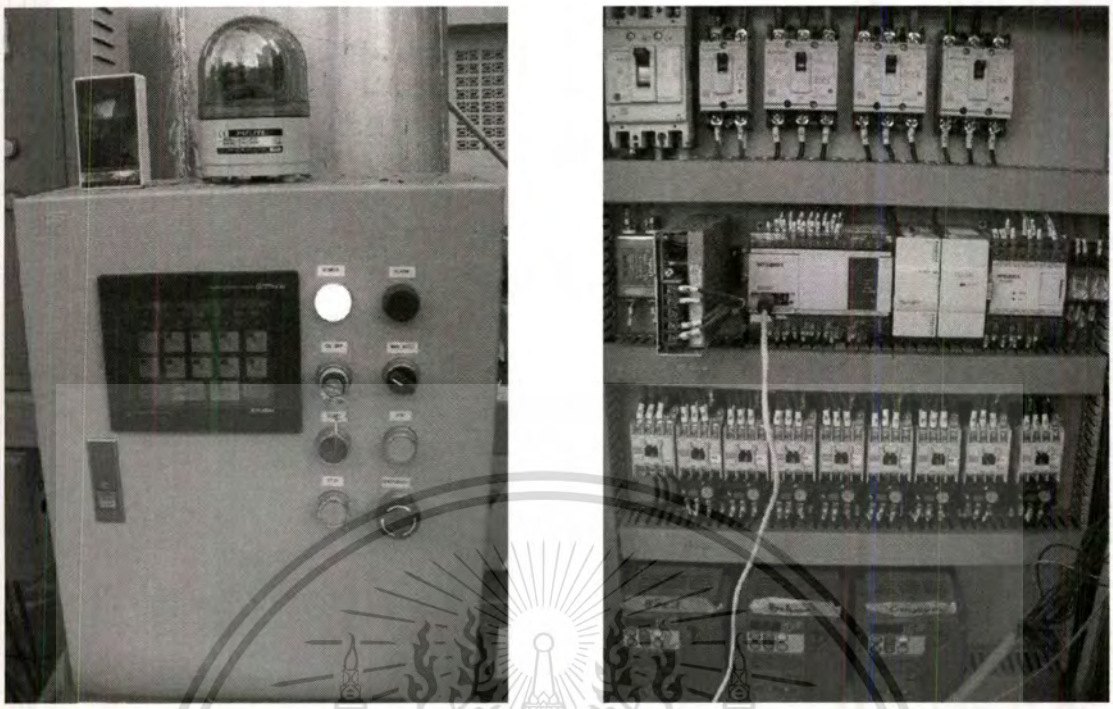

**Fig. b.3** The electrical controller of the microwave carbonization plant

# List of Publications

2012 **Suwilai Areejit**, Poomyos Payakkawan, Anurak Jansri, Kitdakorn Klomkarn, Hisayuki Aoyama and Pitikhate Sooraksa, "Chaotic Application for Industrial Microwave Heating System without Mode-Stirring Mechanism," *International Conference on Microwave and Millimeter Wave Technology (ICMMT2012),* Shenzhen, China, Vol. 5, 5-8 May 2012, pp. 1-3.

2012 Poomyos Payakkawan, **Suwilai Areejit**, Anurak Jansri, Kitdakorn Klomkarn, Hisayuki Aoyama and Pitikhate Sooraksa, "Design and Implementation of Continuous Microwave Biomass Carbonization System," *International Conference on Microwave and Millimeter Wave Technology (ICMMT2012),* Shenzhen, China, Vol. 5, 5-8 May 2012, pp. 1-4.

2013 **Suwilai Areejit**, Pitikhate Sooraksa, and Hisayuki Aoyama "Phase Difference Technique for Material Classification by Using Tuning Fork with Piezoelectric Resonator," *Advanced Materials Research, Trans Tech Publications,* Switzerland, Vol. 750-752, August 2013, pp. 2225-2231.

2013 Poomyos Payakkawan, **Suwilai Areejit**, and Pitikhate Sooraksa "Novel Microwave Carbonization System for Coconut Shells," *Advanced Materials Research, Trans Tech Publications,* Switzerland, Vol. 750-752, August 2013, pp. 1539-1544.

2013 **Suwilai Areejit**, Anurak Jansri, and Pitikhate Sooraksa "Force Sensor and its Application to Tuning Fork Response Measurement," *Advanced Materials Research, Trans Tech Publications*, Switzerland, Vol. 804, September 2013, pp. 222-227.

2014 Poomyos Payakkawan, **Suwilai Areejit**, and Pitikhate Sooraksa "Design, Fabrication and Operation of Continuous Microwave Biomass Carbonization System," *Renewable Energy: An International Journal, ScienceDirect, Elsevier Publishing Solutions*, Vol. 66, June 2014, pp. 49-55.

# Author Biography

Mr. Suwilai Phumpho (formerly Areejit) was born in 1980 in Thailand's Samutprakarn province. In 2003, he graduated summa cum laude with a bachelor's degree in Electronic Engineering from Mahanakorn University of Technology (MUT). In 2008, Mr. Phumpho earned a master's degree in Information Engineering from King Mongkut's Institute of Technology Ladkrabang (KMITL). In addition, he was given a valuable opportunity as a research student to work with and learn from researchers of high caliber at the AOLAB of the Department of Mechanical Engineering and Intelligent Systems, the University of Electro-Communications, Japan, from October to December 2012. With an RGJ grant from the Thailand Research Fund, the author furthered and, in 2014, completed his doctoral degree in Electrical Engineering from the Faculty of Engineering, KMITL. His research interests center around chaotic applications, mechatronic systems, control applications, industrial process control, and renewable energy.